Master's thesis

NTNU
Norwegian University of Science and Technology
Department of Engineering Cybernetics

Bohan Zhang

Smart Grid On-line Impedance Identification

Master's thesis in Master of Science in Cybernetics and Robotics
Supervisor: Marta Maria Cabrera Molinas
June 2019

NTNU
Norwegian University of Science and Technology

Bohan Zhang

Smart Grid On-line Impedance Identification

Master's thesis in Master of Science in Cybernetics and Robotics
Supervisor: Marta Maria Cabrera Molinas
June 2019

Norwegian University of Science and Technology
Department of Engineering Cybernetics

NTNU
Norwegian University of
Science and Technology

Project Description

Name:	Bohan Zhang
Department:	Department of Engineering Cybernetics
Title:	Smart Grid On-line Impedance Identification
Main profile:	Control of smart grids and renewable energy
Start date:	7 January 2019
Due date:	10 June 2019
Supervisor:	Professor Marta Molinas

The purpose of this thesis is to perform an on-line identification of the system impedance based on the identification of harmonics amplitude and phase. Furthermore an injection method is used to analyze the impedance of non-characteristic harmonics.

Work Description:

- Develop equivalent system impedance models based on different operation points.
- Implement an impedance estimation method based on Extended Kalman Filter in Matlab and Simulink.
- Implement an adaptive variant of the Extended Kalman Filter in Matlab and Simulink.
- Implement an impedance estimation method based on Adaptive Kalman Filter in Matlab and Simulink.
- Implement and compare a harmonics linearization mapping method with aforementioned methods.
- Expand Adaptive Kalman Filter capabilities to estimate impedance of non-characteristic harmonics using a signal injection method.
- Conclude the findings of this work.

Abstract

As the current electrical grids are progressing towards SmartGrid, an increasing amount of renewable energy sources and power electronics are connected to the grid. Distortions caused by the nonlinear loads and small inertia of the power source are becoming more severe, and lead to unwanted effects in the system including overheating and reduced component life expectancy. This calls for a way of identifying and accessing these distortions.

The nonlinear distortion consists of harmonics, which are the integer multiples of the grid fundamental frequency. Frequency scanning methods are predominantly used for identifying the harmonics parameters, but have to deal with the time delay caused by the conversion of time domain to frequency domain. There are needs for a real-time identification method that can identify the harmonics impedance which enables further stability assessment of the system.

This thesis analyzes the use of several Kalman filter based on-line identification methods to estimate the harmonics impedance in a rectifier system, including the Extended Kalman Filter(EKF), Adaptive Extended Kalman Filter(AEKF) and Adaptive Kalman Filter(AKF). The results of these method is compared to a impedance mapping method based on harmonics linearization. The AKF yields the most accurate estimation.

To further analyze the impedance of non-characteristic harmonics, we injected the system with a step signal and looked into its transient response. The AKF estimation shows promising results and points to potential use cases in future studies.

Sammendrag

I dag er det en kontinuerlig overgang fra distribuert kraftnettverk til fremtidens Smartnett. Det er en tydelig trend med økende innslag av fornybare energiressurser og kraftelektroniske komponenter i nettverket. Faktorer som ulineære laster og lavt treghetsmomentet fører til økte forstyrrelser i systemet. Det øker risikoen til overoppheting og redusert levetid av nettverkkomponentene. Det er derfor av interesse å måle og identifisere disse forstyrrelsene.

Disse forstyrrelsene består av harmoniske svingninger, som er multipler av grunnfrekvensen. Frekvensskanningsmetoder er ofte brukt for å måle harmoniske svingninger, men lider på grunn av tidsforsinkelsen som skapes ved konverteringen fra tids- til frekvensdomenet. Det er derfor behov for en sanntidsidentifikasjonsmetode som kan måle disse svingningene og muliggjøre en videre stabilitetsevaluering av systemet.

Denne masteroppgaven analyserer flere Kalman-filtre basert på sanntidsidentifikasjonsmetoder i et likerettersystem, blant annet Utvidet Kalman-filtre og Adaptivt Kalman-filtre. Resultatene er sammenlignet med en impedansemodeleringsmetode basert på harmonisk linearisering. Det Adaptive Kalman-filtret gir svært gode resultater.

Videre analyserer basert på ikke-karakteriske harmoniske svingninger. Ved å injisere systemet med en stegfunksjon klarer vi å hente ut informasjon av ikke-karakteriske signalkomponenter fra transientresponsen. Det viser lovende resultater og åpner for videre utvikling og fremtidig forskning av transientanalyse basert impedanseestimering.

Preface

This is the master's thesis to conclude the Master of Science degree in Cybernetics and Robotics at the Norwegian University of Science and Technology. The work was carried out during the spring semester of 2019.

I would first and foremost thank Professor Marta Molinas for the countless guidance and help with this work. I would like to thank Dr.Chen Zhang for providing his insight into the subject of power systems. I would also like to thank Andres Felipe Soler Guevara for his input on implementing the Kalman Filters.

This thesis is dedicated to my friends and family for their endless love and support.

Bohan Zhang
Trondheim, June 2019

Table of Contents

List of Tables

List of Figures

Abbreviations

AEKF	Adaptive Extended Kalman Filter
AKF	Adaptive Kalman Filter
CWT	Continuous Wavelet Transform
DKF	Discrete Kalman Filter
DSP	Digital Signal Processing
EKF	Extended Kalman Filter
EMD	Empirical Mode Decomposition
FFT	Fast Fourier Transform
HHT	Hilbert Huang Transform
IMF	Intrinsic Mode Function
PCC	Point of Common Coupling
STFT	Short Time Fourier Transform
VSC	Voltage Source Converter

Chapter 1

Introduction

1.1 Background

Traditional power supplies consist of power generator with large inertia that makes the grid frequency relatively stable despite sudden changes in the loads. Today electrical grid is gradually transforming toward SmartGrid, with real-world examples like micro-grid, marine vessel grid, solar farm and wind farm. SmartGrids are characterized by high penetration rate of renewable energy sources and non-linear loads such as power electronics and power converters that convert between AC and DC. Combine the non-linearity of the loads with the small inertia of the renewable power generating sources, the grid frequency is more prone to distortions. These distortions contain harmonics, which are often the integer multiples of the fundamental grid frequency(characteristic harmonics). These harmonics cause unwanted effects in the system including overheating and reduced component life expectancy[3]. It is therefore of interest to identify and detect these harmonics signals for the purpose of further stability assessment[4] and harmonics distortion mitigation[5].

Due to the complexity of SmartGrid system especially when the scale grows (e.g. wind farm), high fidelity modeling would not be a sustainable for impedance identification. It contains several different components which interact with each other depending on the control actions and information flow available. Underlying model uncertainties and unknown dynamics make mathematical modeling of SmartGrid a challenging task. This project will work with on-line identification techniques as an alternative to high fidelity modeling. These techniques are based on limited measurement availability and algorithms such as Kalman Filter, which is able to identify critical parameters of the Smart Grid under investigation.

1.2 Project Objective and Design of Experiment

The purpose of this work is to perform an on-line identification of the system impedance based on the identification of harmonics amplitude and phase. Furthermore, an injection method will be used to analyze the impedance of non-characteristic harmonics.

The project will consist of modeling, simulation work (Matlab/Simulink), system identification, signal analysis and impedance estimation. The work will be a mixture of stability theory, signal processing and power system analysis.

1.3 Thesis structure

Chapter 1: Introduction: This chapter presents the background and motivation for the work in this thesis.
Chapter 2: Literature Review: This chapter contains literature review of related topics and work.
Chapter 3: Basic Theory: This section contains a brief presentation of the theoretical background for the terminologies and methods used in this thesis.
Chapter 4: Summary of Previous Work: This chapter is a summary of the work done in the specialization project during Autumn 2018.
Chapter 5: Proposed Parameter Identification Methods: This chapter details the different parameter identification methods for the three-phase rectifier system.
Chapter 6: Transient analysis: This chapter analyzes the system impedance during a transient step response.
Chapter 7: Conclusion and Future Work: Conclusion of the thesis and recommended work for future papers and master thesis.
Appendix A: Matlab Simulink models of the simulated system
Appendix B: Matlab script of the implemented parameter identification methods

Chapter 2

Literature Review

In this chapter some relevant topics and related work are investigated.

2.1 Impedance modeling

On the topic of impedance modeling for three phase diode rectifier, two work stand out. One being Lei(2013)[6], which presents a frequency domain generalized input impedance model. The other work is Bing(2009)[7] which details small-signal input impedance analysis based on harmonic linearization mapping method.

2.2 Impedance Identification

Impedance identification can be achieved by offline frequency-response analysis. Different frequency domain identification methods are presented and compared in the previous specialization project, summarized in **Chap 4**. Frequency scanning methods have the disadvantage of having a time delay due to the conversion of time domain to frequency domain.

Examples of passive methods can be found in papers such as Hoffmann(2014)[8], Jondal(2017)[9], Sanchez(2015)[10] and Broen(2016)[11]. These methods are designed to utilize the disturbances that are already present in typical power networks and are less invasive to the system. They provide real-time estimation of the equivalent grid impedance by means of recursive estimation techniques such as Kalman Filter. One challenge for these passive methods is for example tuning the filter.

On the other side there are also active methods, such as the ones proposed in Sumner(2002) [12] and Asiminoaei(2004)[13]. These techniques utilize a forced disturbance that is injected as a perturbation current or voltage. Based on the injection signal, these methods are able to determine the grid impedance at individual frequencies or in characteristic frequency bands. Small signal injection frequency response analysis is accurate but off-line, and in most cases invasive to the system.

2.3 Stability Analysis

Small-signal impedance stability analysis for power electronics systems is discussed in papers such as Sun(2011) [4] and Amin(2019) [14]. Both apply *Nyquist Stability Criterion* on small-signal impedance models. In contrast to the small-signal method are the large-signal stability analysis which are detailed in Griffo(2008)[15] and Sanchez(2015)[10].

Chapter 3

Basic Theory

This chapter contains a brief presentation of the theoretical background for the terminologies and methods used in this thesis.

3.1 Diode bridge rectifier

Diode rectifiers are commonly used for converting an AC input supply into a DC supply. It gained popularity due to its affordability and the ability of handling high voltage. There are single phase(as shown in **Fig 3.1**) and three-phase diode bridge rectifiers(as shown in **Fig 3.2**), where the three-phase variant is more preferable due to the low ripple content in the wave-forms and a higher power handling capability[1, P.103]. It utilizes diode bridge for the rectification process, which constitutes as a non-linear load. Current drawn by the nonlinear loads such as the diode bridge rectifier results in distortions and harmonics in the system.

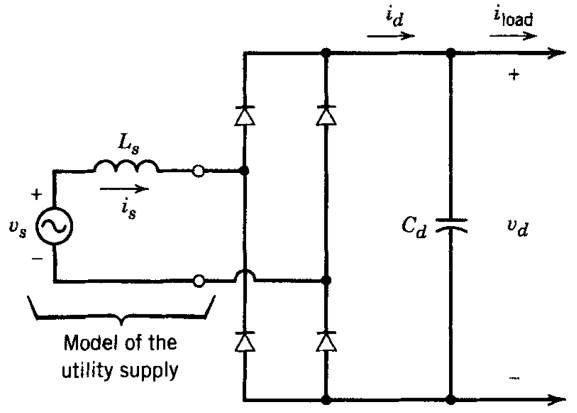

Figure 3.1: Single-phase diode bridge rectifier [1, P.83]

3.1.1 Three-phase diode rectifier characteristic

Fig 3.2 shows an example of the three-phase, six-pulse full bridge rectifier.

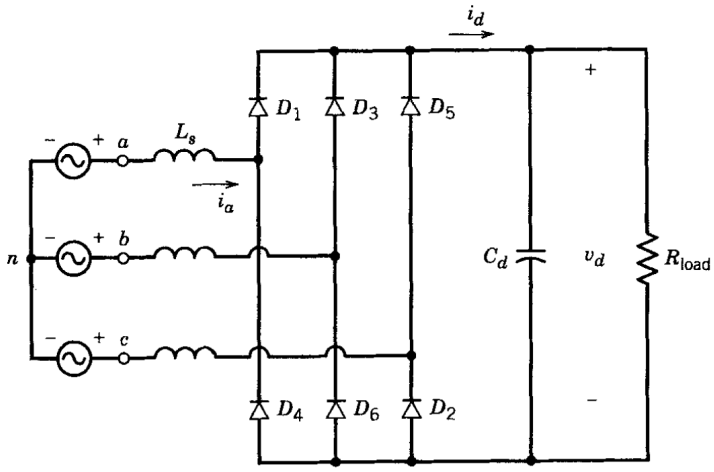

Figure 3.2: Three-phase full bridge rectifier [1, P.103]

From Lei's input impedance modeling of three-phase diode rectifier[6], the equivalent output dc voltage v_d and the input three-phase voltages are related by the switching function S_a, S_b, and S_c:

$$v_d = v_a S_a + v_b S_b + v_c S_c \tag{3.1}$$

S_a, S_b, and S_c are all stair switching functions, and can be decoupled into infinite number of sinusoidal wave-forms with multiple times of fundamental frequencies, so called the Fourier series:

$$S_a = \sum_{n=1}^{\infty} (A_{sn} cos(n\theta) + B_{sn} sin(n\theta)) \tag{3.2}$$

Where the coefficient is defines as:

$$A_{sn} = \frac{2\sqrt{3}(-1)^l}{\pi} \frac{\sin n(u+\phi) + sin(n\phi)}{n} \tag{3.3a}$$

$$B_{sn} = \frac{2\sqrt{3}(-1)^l}{\pi} \frac{\cos n(u+\phi) + cos(n\phi)}{n} \tag{3.3b}$$

$$n = 6l \pm 1 (l = 0, 1, 2, 3, \ldots n > 0) \tag{3.3c}$$

We observe that the sinusoidal in the coefficient is of order $n = 6l \pm 1$, which indicates that this is the characteristic harmonics of the AC voltage. Subsequently the AC current will have the same characteristic harmonics in its content.

3.2 Harmonics

In the context of power systems, a harmonic is defined as the content of the electronic signal whose frequency is an integer multiple of the system fundamental frequency, which is commonly 50 Hz in Europe and 60 Hz in the US [16, p.1]. Harmonics emerges when there are non-linear loads in the system, such as rectifiers and switching power supplies. Applying voltage to these non-linear loads will result in complex current waveform, which according to Fourier analysis(**Ch 3.4**) can be decomposed into integer multiples of the fundamental frequency.

3.3 Superposition Principle

Superposition Principle states that for linear systems the response causes by multiple sources is equivalent to the algebraic sum of each individual source responses. Voltage and current are sinusoidal signals, and according to Fourier Analysis each can be decomposed into infinite many sinusoids. Each sinusoid will then have their own impedance responses, which can be analyses individually. This allow us to decompose our voltage and current signals into subsequent harmonics and compute their impedance individually.

3.4 Fourier Analysis

The analysis and modeling of the harmonics are largely based on the Fourier analysis, which states that every non-sinusoidal periodic wave can be decomposed as the sum of sine waves through the application of the Fourier series[17]. This gives the basis for the harmonic measurement methods[18]:

$$x(t) = a_0 + \sum_{h=1}^{\infty} c_h \sin(\frac{h}{N}\omega_n t + \phi_h) \tag{3.4a}$$

$$c_h = \sqrt{a_h^2 + b_h^2} \tag{3.4b}$$

$$\phi_h = \tan^{-1}\frac{a_h}{b_h}, if b_h \geq 0 \tag{3.4c}$$

$$\phi_h = \pi + \tan^{-1}\frac{a_h}{b_h}, if b_h < 0 \tag{3.4d}$$

ω_n is the fundamental frequency, h is the harmonic order and N is the number of samples of a period of the signal. a_h and b_h are the harmonics' phasor(Eulers' identity) component:

$$a_h = \frac{2}{T_\omega}\int_0^{T_\omega} x(t)\cos(\frac{h}{N}\omega_n t + \phi_h)dt \tag{3.5a}$$

$$b_h = \frac{2}{T_\omega}\int_0^{T_\omega} x(t)\sin(\frac{h}{N}\omega_n t + \phi_h)dt \tag{3.5b}$$

$$a_0 = \frac{1}{T_\omega} \int_0^{T_\omega} x(t)dt \tag{3.5c}$$

where T_ω is the window width.

3.5 Fast Fourier Transform

Fast Fourier Transform (FFT) is a divide and conquer algorithm which computes the discrete *Fourier Transform*:

$$\hat{x} = \sum_{n=0}^{N-1} x_n e^{-\frac{2\pi j}{N} kn} \tag{3.6}$$

of a sequence x of length N, and transforms it from the time domain into frequency domain. The signal gets decomposed into sinusoidal frequency components, which gives us an overview of the frequencies that is present in the signal. FFT is most suitable for stationary signals as any change in the frequency components will get diluted. The major frequency components of the original sequence can be observed from the energy spectral density of x:

$$S_{xx}(f) = |\hat{x}(f)|^2 \tag{3.7}$$

3.6 Short-Time Fourier Transform

$$X(t, f) = \int_{-\infty}^{\infty} x(t_1)h^*(t_1 - t)e^{-i2\pi f t_1} dt_1 \tag{3.8}$$

The *Short-Time Fourier Transform* (STFT) uses a window function h(t) that divides the signal into shorter windows, and then compute the Fourier transform of each windows. STFT is suitable for slowly varying non-stationary signals, because the signal can be considered stationary in a small enough window. There will however be a trade-off between time and frequency resolution according to the *Uncertainty Principle* [19]. A *spectrogram* contains the spectral density of each window:

$$S_{xx}(t, f) = |X(t, f)|^2 \tag{3.9}$$

3.7 Continuous Wavelet Transform

Continuous wavelet transform (CWT) computes a convolution of the signal with the scaled wavelet Φ where the scale $|a|$ changes continuously. The scale only changes the duration and the bandwidth of the wavelet without changing its shape. The CWT of a time-series $x(t)$ is given by:

$$\hat{x}(t, a) = \int_{-\infty}^{+\infty} x(\tau)|a|^{-1/2}\Phi\left(\frac{\tau - t}{a}\right)d\tau \tag{3.10}$$

CWT differs from STFT in that it uses short windows at high frequencies and long windows at low frequencies, instead of using one single analysis window like STFT [20].

3.8 Symmetrical Component Transformation

In able to utilize the *Kalman Filter*(KF) the system have to be transformed into state-space form. The unbalanced three-phase system is first transformed into three balanced systems named the positive, negative and zero sequence by using the *Fortescue Theorem*. And then the three-phase signal is simplified by *Clarke transform* which project the system onto $\alpha\beta$ stationary frame.

3.8.1 Fortescue Theorem

Fortescue theorem states that 3 unbalanced phasors of a 3-phase system can be resolved into 3 balanced systems of phasors:

$$\begin{aligned} V_a &= V_{a,p} + V_{a,n} + V_{a,0} \\ V_b &= V_{b,p} + V_{b,n} + V_{b,0} \\ V_c &= V_{c,p} + V_{c,n} + V_{c,0} \end{aligned} \tag{3.11}$$

Eq 3.11 shows the three-phase unbalanced system V_{abc} transformed into three balanced sequence components. $V_p = [V_{a,p}, V_{b,p}, V_{c,p}]^T$ is the positive sequence, where the components have the same magnitude and is displaced by 120°with each other.
$V_n = [V_{a,n}, V_{b,n}, V_{c,n}]^T$ is the negative sequence. The components in the negative sequence also have the same magnitude while in a displacement of 120°with each other, but in the opposite phase sequence than of the positive sequence. $V_0 = [V_{a,0}, V_{b,0}, V_{c,0}]^T$ is the zero sequence, where components are balanced and in phase with each other. A balanced system has the advantage of reduced required states and the system complexity.

3.8.2 Clarke Transform

Clarke transformation($\alpha\beta0$ transformation) projects the three-phase system onto the $\alpha\beta$ stationary frame by using the transformation matrix:

$$T_{\alpha\beta0} = \frac{2}{3}\begin{bmatrix} 1 & -\frac{1}{2} & -\frac{1}{2} \\ 0 & \frac{\sqrt{3}}{2} & -\frac{\sqrt{3}}{2} \\ \frac{1}{2} & \frac{1}{2} & \frac{1}{2} \end{bmatrix} \tag{3.12}$$

When applying Clarke transform to a balanced three-phase system, the 0 component becomes zero. The transformation matrix can therefore be simplified as:

$$T_{\alpha\beta} = \frac{2}{3}\begin{bmatrix} 1 & -\frac{1}{2} & -\frac{1}{2} \\ 0 & \frac{\sqrt{3}}{2} & -\frac{\sqrt{3}}{2} \end{bmatrix} \tag{3.13}$$

3.9 Discrete Kalman Filter

Kalman filter can be described as an recursive algorithm that enables "linear time-domain minimum mean-square error filtering."[2, p.141-147] It is a well established method within the realm of state estimation and tracking. To apply the *Discrete Kalman Filter*(DKF), the system has to be in discrete time and state-space form:

$$\begin{aligned} X_{k+1} &= \Phi_k X_k + W_k \\ Z_k &= H_k X_k + V_k \end{aligned} \tag{3.14}$$

Here X_k is the state vector, Φ_k is the state-transition matrix, Z_k is the measurement vector and H_k is measurement matrix. W_k and V_k are respectively the process noise and measurement noise.
We start with the a priori estimate $\hat{X}_k^-$ and try to improve it with the measurement Z_k:

$$\hat{X}_k = \hat{X}_k^- + K_k(Z_k - H_k\hat{X}_k^-) \tag{3.15}$$

The Kalman gain K_k minimizes the mean-square estimation error which is obtained through:

$$K_k = P_k^- H_k^T (H_k P_k^- H_k^T + R_k)^{-1} \tag{3.16}$$

Update the error covariance from the a priori P_k^-:

$$P_k = (I - K_k H_k) P_k^- \tag{3.17}$$

The we predict the state vector and the error covariance ahead:

$$\begin{aligned} \hat{X}_{k+1}^- &= \Phi_k \hat{X}_k \\ P_{k+1}^- &= \Phi_k P_k \Phi_k^T + Q_k \end{aligned} \tag{3.18}$$

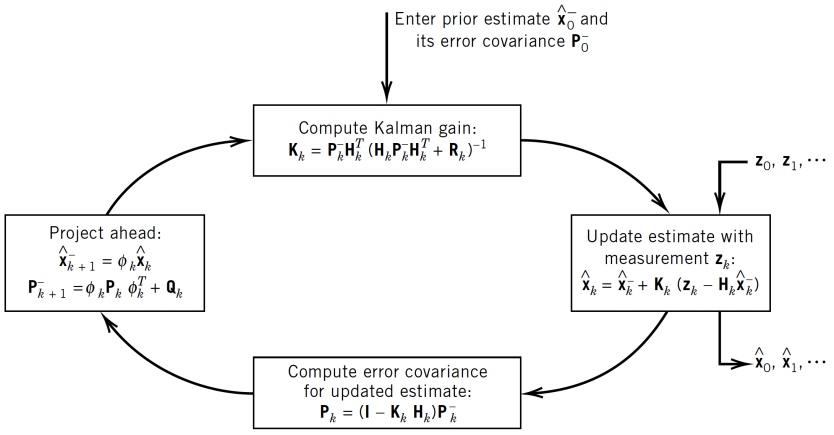

Figure 3.3: Kalman Filter loop [2, P.147]

3.10 Extended Kalman Filter

Most real life system are considered non-linear, which makes the Kalman Filter described in section 3.9 not applicable. For non-linear systems, one could us Extended Kalman Filter for parameter estimation, which is established in [21, p.547-549]. We can write the non-linear system models as:

$$\begin{aligned} x_{k+1} &= f_k(x_k, u_k) + \epsilon_k \\ y_k &= g_k(x_k) + \nu_k \end{aligned} \tag{3.19}$$

The prediction step for the a priori states is hence given as:

$$\hat{x}_{k+1}^- = f_k(\hat{x}_k, u_k) \tag{3.20}$$

For each step the Jacobian matrices are calculated as:

$$F_k = \frac{\partial f_k(x,u)}{\partial x}\Big|_{x=\hat{x}_k, u=u_k} \tag{3.21}$$

$$G_{k+1} = \frac{\partial g_{k+1}(x)}{\partial x}\Big|_{x=\hat{x}_{k+1}^-} \tag{3.22}$$

The a priori error covariance is predicted as:

$$P_{k+1}^- = F_k P_k F_k^T + Q_k \tag{3.23}$$

And the Kalman gain is calculated as:

$$K_{k+1} = P_{k+1}^- G_{k+1} (G_{k+1} P_{k+1}^- G_{k+1}^T + R_k)^{-1} \tag{3.24}$$

Update the a posteriori system states and error covariance:

$$\hat{x}_{k+1} = \hat{x}_{k+1}^- + K_{k+1}(y_{k+1} - g_{k+1}(\hat{x}_{k+1}^-)) \tag{3.25}$$

$$P_{k+1} = (I - K_{k+1} G_{k+1}) P_{k+1}^- \tag{3.26}$$

In the fashion of the original Kalman Filter, these steps(Equation 3.20- Equation 3.26) are also repeated recursively. With the right tuning it will achieve an accurate state estimation even with distortions and noise in the measurements. It greatly reduces the calculation burden and provides a way of parameter estimation in non-linear systems.

3.11 Adaptive Kalman Filter

The concept of an Adaptive Kalman filter was established in [22], which is further improved by Anders in [11, p.23] by including a maximum number of iterations for updating

the Q:

$q^- = q[k-1];$
$Q[k] = q^- I;$
while $i \neq N$ **do**
  $P^-[k] = AP[k-1]A^T + Q[k];$
  $K[k] = P^-[k]C[k]^T(C[k]P^-C[k]^T + R)^{-1};$
  $\hat{X}[k] = \hat{X}^-[k] + K[k](y[k] - C[k]\hat{X}^-[k]);$
  $\hat{W}[k] = K[k](y[k] - C[k]\hat{X}^-[k]);$
  $q = \frac{1}{n}\sum_i^n \hat{w}_i[k]^2;$
  if $|q| - |q^-| < \epsilon$ **then**
    break;
  end
  $Q[k] = qI;$
  $q^- = q;$
  $i+ = 1;$
end
$P[k] = (I - K[k]C[k]P^-[k]);$

Algorithm 1: AKF algorithm

This algorithm is adaptive in the sense that the error covariance is calculated for each iteration, which gets an improved estimate of the state compared to having just a constant error covariance.

3.12 Sequence Analysis

Sequence analysis is enabled through the *Sequence Analyzer* block in Simulink. It applies Fourier analysis to the three input signals over a sliding window of one cycle of the specified frequency. It evaluates the phasor values Va, Vb, and Vc at the specified fundamental or harmonic frequency. Then the transformation is applied to obtain the positive sequence, negative sequence, and zero sequence. Sequence Analyzer block outputs the magnitude and phase of the positive-, negative-, and zero-sequence components of a set of three balanced or unbalanced signals. Index 1 denotes the positive sequence, index 2 denotes the negative sequence, and index 0 denotes the zero sequence. The signals can optionally contain harmonics.

$$\begin{aligned} V_1 &= \frac{1}{3}(V_a + a \cdot V_b + a^2 \cdot V_c) \\ V_2 &= \frac{1}{3}(V_a + a^2 \cdot V_b + a \cdot V_c) \\ V_0 &= \frac{1}{3}(V_a + V_b + V_c) \end{aligned} \tag{3.27}$$

Where Va, Vb, Vc are the three voltage phasors at the specified frequency, and a=$e^{j2\pi/3}$ =1$\angle$120 is the complex operator.

3.13 Genetic Algorithm

The genetic algorithm is a method for solving optimization problems that is inspired by the process of natural selection. Selection of solution(population) relies on three genetic algorithms: elitism, crossover and mutation. By starting off with an initial population, we apply the genetic algorithms for generations until the population has converged, meaning that the newly produce solution(offspring) does not differs significantly from previous solutions(parents).

3.14 Real-Time

Real-time in the context of system estimation and computing means that it has guaranteed or predictable response time. It is characterized by high reliability and efficiency and limited computational load for each step.

3.15 Generalized Nyquist Stability Criterion

The generalized Nyquist stability criterion is introduced Desoer(1980) [23] and later established as a impedance-based stability analysis method in Sun(2011) [4]. By defining the system in a source and a load subsystem, the transfer function from the source voltage to the load voltage can be written as:

$$H(s) = \frac{V_S(s)}{V_{load}(s)} = \frac{1}{1 + \frac{Z_S(s)}{Z_{load}(s)}} \tag{3.28}$$

The interconnected source-load system stability can be then determined by applying the Nyquist stability criterion to the ratio between the source output impedance Z_S and the load input impedance Z_{load}. The system is stable if the Nyquist plot of the impedance ratio does not have any encirclement of the point -1. It can also be calculated by finding ω_{180} that make $\angle \frac{Z_S(j\omega_{180})}{Z_{load}(j\omega_{180})} = -180°$ and check if $|\frac{Z_S(j\omega_{180})}{Z_{load}(j\omega_{180})}| < 1$ [24].

Chapter 4

Summary of Previous Work

This thesis is a continuation of the specialization project *Smart grid parameter identification Methods* of fall 2018, which established that AKF is a fitting method for harmonics parameter identification. This chapter includes the main results and findings of the specialization project.

The specialization project *Smart grid parameter identification Methods* studied the use of *Fast Fourier Transform*, *Short-Time Fourier Transform*, *Continuous Wavelet Transform*, *Hilbert-Huang Transform*, and *Adaptive Kalman Filter* for parameter identification of the harmonics. These methods are tested on both synthetic composite signal and complex smart grid signal.

4.1 Synthetic Composite Signal

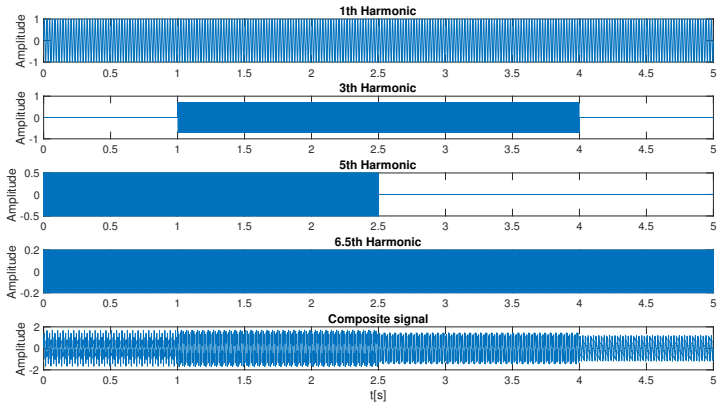

Figure 4.1: The harmonic signal components and the composite signal that contains them.

The synthetic composite signal in **Fig 4.1** contains the 1th(the fundamental frequency), 3th(intermittent), 5th(intermittent) and the 6.5th(non-characteristic) harmonics.

As seen in **Fig 4.2**, the FFT were excellent in pinpointing the exact frequency of the components, but unable to extract the time information of the intermittent signals. STFT and CWT are similar in that both visualizes the components in time and frequency spectrum. STFT do suffers a time and frequency accuracy trade off, which is problematic for non-stationary signals. CWT does not suffer from this time-frequency trade off but choosing a fitting wavelet could be a challenge. Additionally, CWT suffers from the "edge effect" which could potentially cause information loss at the start and end of the signal.

The AKF requires more prior knowledge about the system than the other methods. The parameter such as fundamental frequency, initial input co-variance, orders of harmonics etc has to be known in order to initialize the AKF. In return the AFK performs very well, especially with capturing the dynamics in the signals(**Fig 4.3**). Additionally it is able to provides the magnitude and phase angle of each component in real time, which is desired property for system monitoring and control.

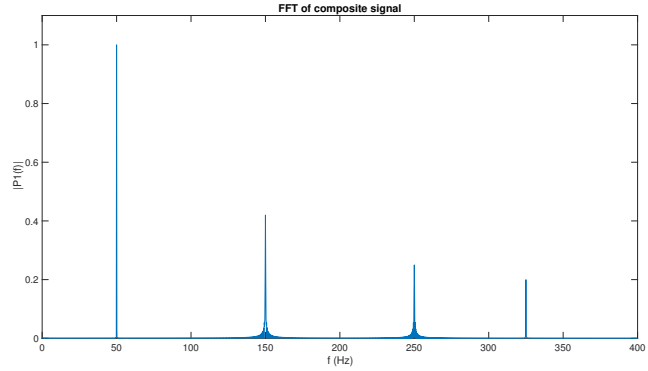

Figure 4.2: The FFT of the composite signal.

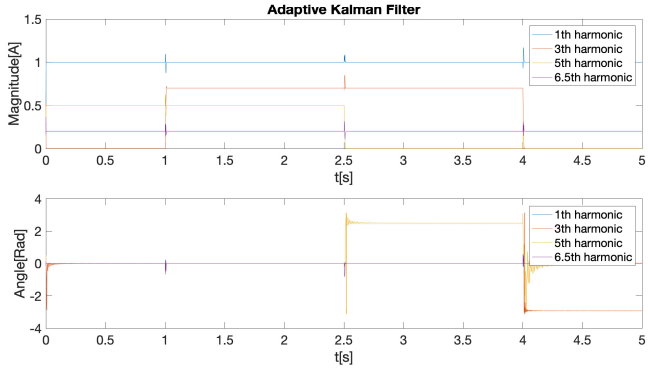

Figure 4.3: Magnitude and phase angle of the identified harmonics for the synthetic signal.

4.2 Complex Smart Grid Signal

The methods were tested further by applying them to signal data from simulation of a complex smart grid system. **Fig 4.4** shows the part of the system that is being analyzed, which is powered by distributed DC power sources. These DC sources are then converted to AC through a single three-phase Voltage Source Converter (VSC), which has a switching frequency of 2.85 kHz. Measurements are done at the PCC on the AC side, where the three-phase current and voltage are sampled at 10kHz for a duration of 4 seconds. The system is stabilized and is therefore stationary. The three phases signal is also balanced and noise free.

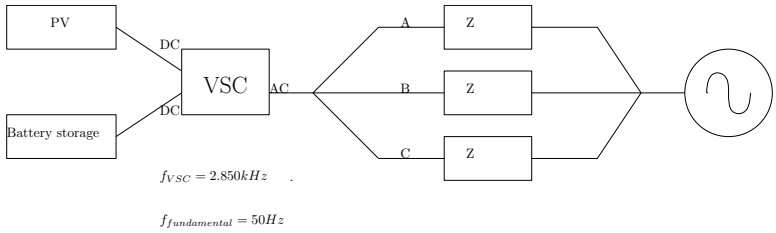

Figure 4.4: Grid schematics. The grid is supplied by DC sources that is converted to AC through the VSC.

Fig 4.5 reveals that the most significant components varies for the voltage and current signal. Beside the 1th order harmonic, 55th, 59th, 85th and the 87th order harmonics are significant in both voltage and current, which gives us the basis to focus on these four harmonics later in the AKF.

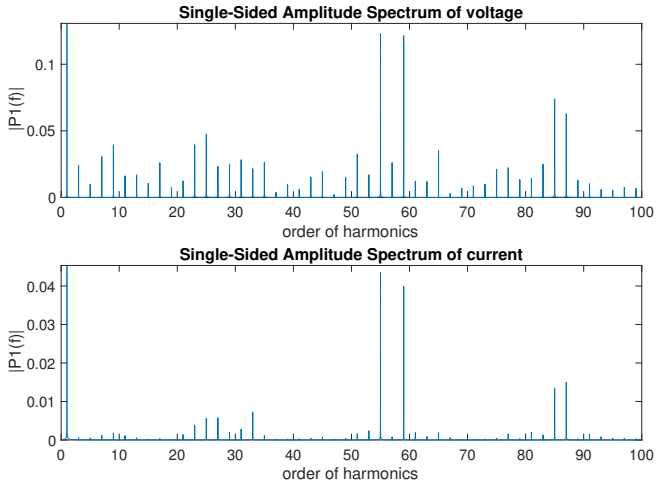

Figure 4.5: FFT of the grid voltage and current with the x-axes showing the order of the harmonics.

Due to the drastic difference between the fundamental frequency magnitude and the rest of the frequency components, both STFT and CWT failed to visualize the harmonics

in the current signal with linear scaling. For STFT this can be resolved by using a logarithmic scaling instead. However, the logarithmic scaling makes it difficult to pinpoint the exact magnitude of the signals.

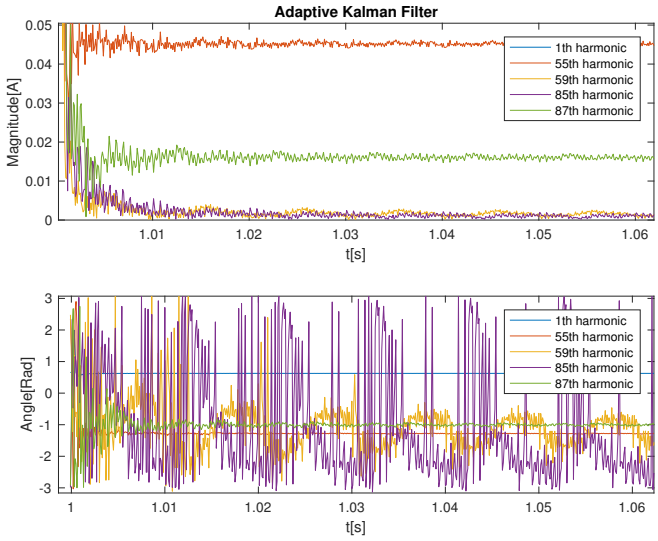

Figure 4.6: Zooming in on the magnitude of higher order harmonics detected in the grid current using the AKD. The measurement covariance $R = 10^{-3}$

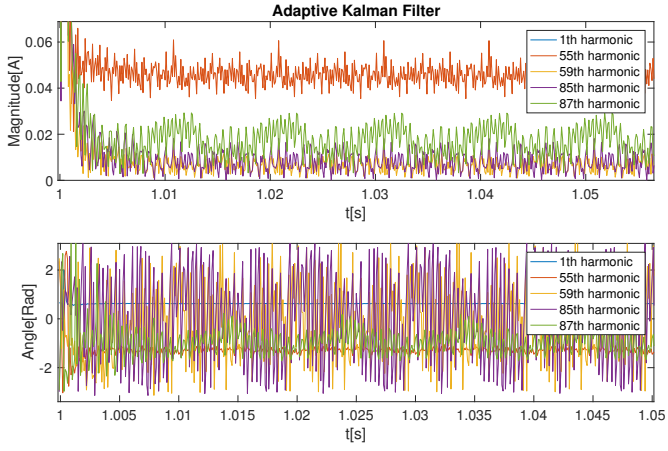

Figure 4.7: Magnitude of higher order harmonics detected in the grid current using the AKF with measurement covariance $R = 10^{-4}$

The AKF performed well and is able to give us the magnitude and phase angle of the specific harmonics it is tracking. Among all the methods tested AKF requires the most

amount of priori knowledge about the signal, such as orders of the harmonics, measurement covariance matrix and initial error covariance matrix. Tuning the parameters of the AKF could be a challenge as seen in **Fig 4.6** and **Fig 4.7**, the initialized value plays a big roll in its performance.

4.3 Methods Viability for Stability Analysis

Considering the aspect of parameter identification, the AKF performed the best among all the methods tested. It is responsive and has the added bonus of providing the harmonics phase angle. If we can overcome the challenge of tuning and initializing the AKF, it is very much suitable for stability analysis.

Furthermore, AKF is an on-line method, meaning it runs in real time. It has the benefit of detecting abnormalities in the system without delay and gives ground to on-line stability analysis. By following the superposition principle, we can use AKF to identify each harmonic in both voltage and current, and divide them through complex division to obtain individual impedance:

$$Z_{ith} = \frac{V_{ith}}{I_{ith}} \tag{4.1}$$

Where *i* is the order of the harmonics.

Chapter 5

Proposed Parameter Identification Methods

In this chapter two operation points is defined for our system, and parameter identification methods for respective operation points are developed. For the operation point on the three-phase bus, Exended Kalman Filter(and it adaptive variant) and Adaptive Kalman Filter is utilized. While for the operation point on the DC bus, a harmonics modeling method is utilized.

For our experiments we are analyzing the three-phase diode bridge rectifier, which are one of the most commonly used devices in power systems. It is often used for battery charger. It consists of three parts: the three-phase source, diode bridge and the DC load Z_{dc}, where the diode bridge together with Z_{dc} makes up the load subsystem. This is a typical source—load system, and is suitable for applying Nyquist stability criterion to study its stability. The three phases are assumed to be balanced.

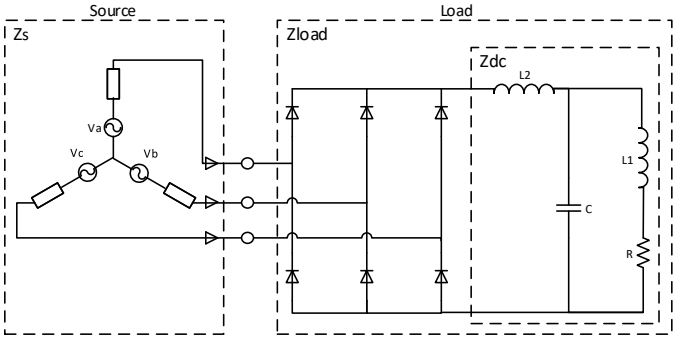

Figure 5.1: Three phase diode rectifier system model.

The initialized value for the system elements are shown in **Tab 5.1**.

Component	Value
L1	$5 \times 10^{-3} H$
L2	$5 \times 10^{-3} H$
C	$3 \times 10^{-4} F$
R	10Ω

Table 5.1: System components values

The following sections will propose different methods of obtaining the impedance of the source and load subsystems.

5.1 Using the Three Phase PCC As the Operation Point

Fig 5.2 shows the equivalent system model of the three-phase rectifier. We use the three-phase bus between the three-phase source and the diode bridge as the Point of Common Coupling(PCC),

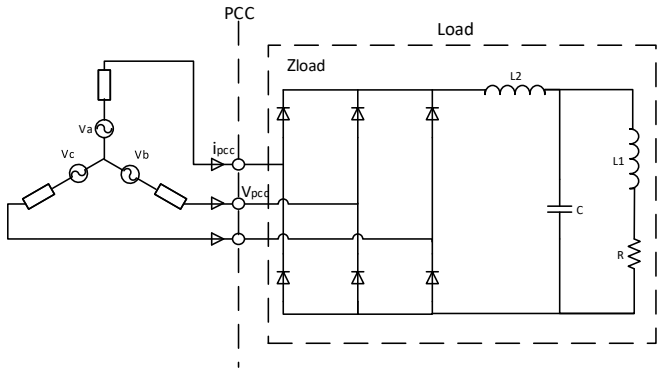

Figure 5.2: Equivalent system impedance model with the operation point at the AC side.

The measurements at the PCC are taken after the system is in steady state.

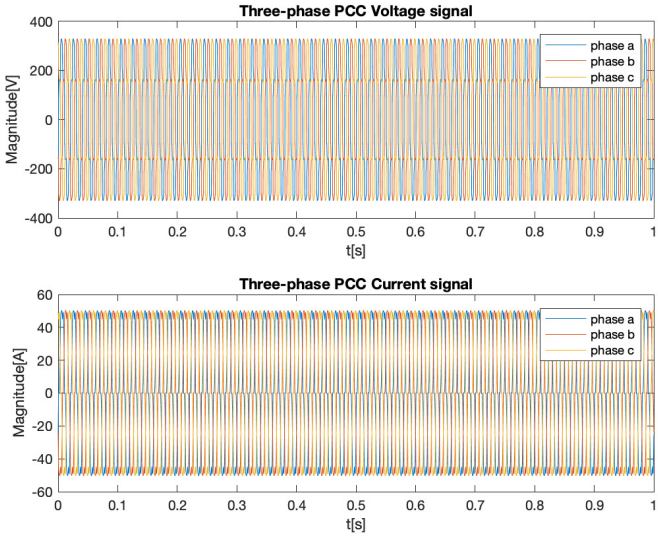

Figure 5.3: The measured three-phase PCC voltage and current signal.

The 6-pulse rectifier has harmonics naturally embedded in it as seen in **Sec 3.1.1**, which are in the order of $6k f_{nom} \pm 1$. Doing a FFT analysis on the voltage signal also quickly reveals the underlying harmonics.

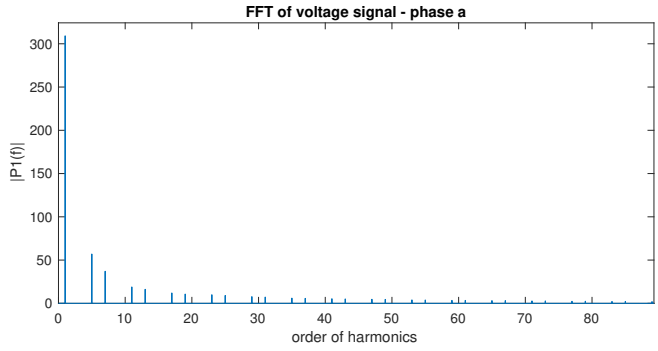

Figure 5.4: The FFT of voltage signal.

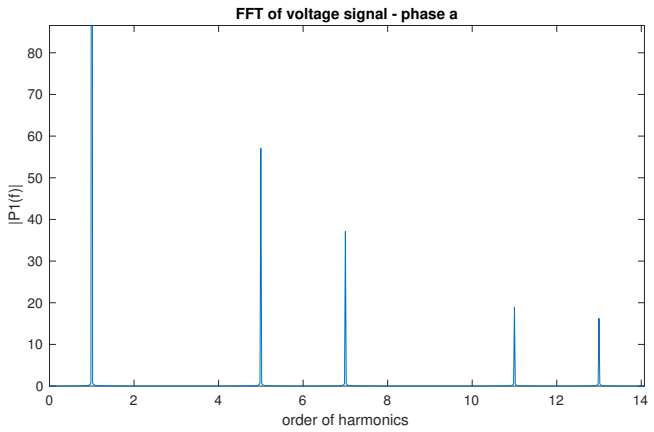

Figure 5.5: The lower order harmonics of voltage signal.

Fig 5.4 shows that the magnitude of the harmonics decreases with the increase of its order. This means that the lower order harmonics(**Fig 5.5**) are the most critical for the states estimation.

5.1.1 Parameter Estimation based on Extended Kalman Filter

Hoffmann(2014)[8] introduced a parameter estimation method based on Extended Kalman Filter(EKF). It aims to utilize the non-linear property of EKF to perform a minimal invasive impedance estimation on a time-variant and frequency-dependent power system, which consists of non-linear loads.

In Hoffmann's paper, the system is modeled to estimate the source output impedance Z_s, where as for our system we want to estimate the load input impedance Z_{load}. For our estimation the changes in the system model is reflected in the One-line diagram seen in **Fig 5.6**. Thevenin equivalent is used to derive this equivalent system impedance model. This diagram shows the equivalent three-phase diode rectifier system impedance seen from the connection point(PCC) of the overall network. The source output impedance (Z_s) can be derived separately using the analytical impedance model.

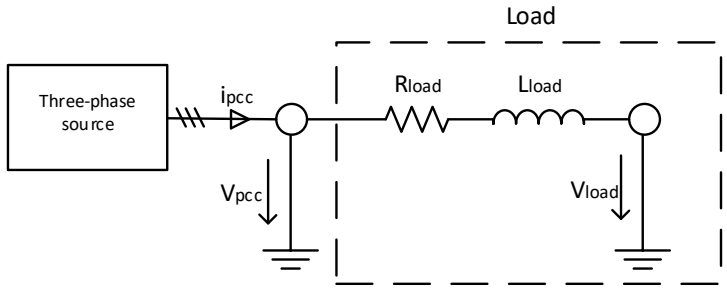

Figure 5.6: One-line diagram of the equivalent system impedance model.

From the diagram, we can deduct the equation below:

$$L_S \frac{di_{pcc}}{dt} + R_S i_{pcc} = V_{pcc} - V_{load} \tag{5.1a}$$

$$L_S \frac{di_{pcc}}{dt} = -R_S i_{pcc} + V_{pcc} - V_{load} \tag{5.1b}$$

$$\frac{di_{pcc}}{dt} = -\frac{R_S}{L_S} i_{pcc} + \frac{V_{pcc}}{L_S} - \frac{V_{load}}{L_S} \tag{5.1c}$$

Which in $\alpha\beta$ frame becomes:

$$\frac{d}{dt}\begin{bmatrix} i_{pcc,\alpha} \\ i_{pcc,\beta} \end{bmatrix} = \begin{bmatrix} -\frac{R_S}{L_S} & 0 \\ 0 & -\frac{R_S}{L_S} \end{bmatrix} \begin{bmatrix} i_{pcc,\alpha} \\ i_{pcc,\beta} \end{bmatrix} + \begin{bmatrix} \frac{1}{L_S} & 0 \\ 0 & \frac{1}{L_S} \end{bmatrix} \begin{bmatrix} V_{pcc,\alpha} \\ V_{pcc,\beta} \end{bmatrix} + \begin{bmatrix} -\frac{1}{L_S} & 0 \\ 0 & -\frac{1}{L_S} \end{bmatrix} \begin{bmatrix} V_{load,\alpha} \\ V_{load,\beta} \end{bmatrix} \tag{5.2}$$

Following the observer reformulation we obtain:

$$\frac{d}{dt}\begin{bmatrix} i_{pcc,\alpha} \\ i_{pcc,\beta} \\ V_{pcc,\alpha} \\ V_{pcc,\beta} \\ V_{load,\alpha} \\ V_{load,\beta} \end{bmatrix} = \underbrace{\begin{bmatrix} -\frac{R_S}{L_S} & 0 & \frac{1}{L_S} & 0 & -\frac{1}{L_S} & 0 \\ 0 & -\frac{R_S}{L_S} & 0 & \frac{1}{L_S} & 0 & -\frac{1}{L_S} \\ 0 & 0 & 0 & 0 & 0 & 0 \\ 0 & 0 & 0 & 0 & 0 & 0 \\ 0 & 0 & 0 & 0 & 0 & 0 \\ 0 & 0 & 0 & 0 & 0 & 0 \end{bmatrix}}_{:=A} \begin{bmatrix} i_{pcc,\alpha} \\ i_{pcc,\beta} \\ V_{pcc,\alpha} \\ V_{pcc,\beta} \\ V_{load,\alpha} \\ V_{load,\beta} \end{bmatrix} \tag{5.3}$$

And the measurement vector is:

$$y = \begin{bmatrix} i_{pcc,\alpha} \\ i_{pcc,\beta} \\ V_{pcc,\alpha} \\ V_{pcc,\beta} \end{bmatrix} = \underbrace{\begin{bmatrix} 1 & 0 & 0 & 0 & 0 & 0 \\ 0 & 1 & 0 & 0 & 0 & 0 \\ 0 & 0 & 1 & 0 & 0 & 0 \\ 0 & 0 & 0 & 1 & 0 & 0 \end{bmatrix}}_{=G} \begin{bmatrix} i_{pcc,\alpha} \\ i_{pcc,\beta} \\ V_{pcc,\alpha} \\ V_{pcc,\beta} \\ V_{load,\alpha} \\ V_{load,\beta} \end{bmatrix} \tag{5.4}$$

Through superposition the equivalent Load subsystem voltage V_{load} is modeled using the harmonics: positive and negative sequence fundamental voltage $V_{S,1+}$ and $V_{S,1-}$; 5th harmonic $V_{S,5-}$(negative sequence); And 7th harmonic $V_{S,7+}$(positive sequence). The final discretizied state space formulation with the extended disturbance model is:

$$\begin{bmatrix} i_{pcc,\alpha}(k+1) \\ i_{pcc,\beta}(k+1) \\ V_{pcc,\alpha}(k+1) \\ V_{pcc,\beta}(k+1) \\ V_{load1+,\alpha}(k+1) \\ V_{load1+,\beta}(k+1) \\ V_{load1-,\alpha}(k+1) \\ V_{load1-,\beta}(k+1) \\ V_{load5-,\alpha}(k+1) \\ V_{load5-,\beta}(k+1) \\ V_{load7+,\alpha}(k+1) \\ V_{load7+,\beta}(k+1) \\ R_{load}(k+1) \\ L_{load}(k+1) \end{bmatrix} = \underbrace{\begin{bmatrix} [1 - T_S\frac{R_{load}(k)}{L_{load}(k)}]i_{pcc,\alpha}(k) - \frac{T_S}{L_{load}(k)}V_{pcc,\alpha}(k) + \frac{T_S}{L_{load}(k)}[V_{load1+,\alpha}(k) + V_{load1-,\alpha}(k) + V_{load5-,\alpha}(k) + V_{load7+,\alpha}(k)] \\ [1 - T_S\frac{R_{load}(k)}{L_{load}(k)}]i_{pcc,\beta}(k) - \frac{T_S}{L_{load}(k)}V_{pcc,\beta}(k) + \frac{T_S}{L_{load}(k)}[V_{load1+,\beta}(k) + V_{load1-,\beta}(k) + V_{load5-,\beta}(k) + V_{load7+,\beta}(k)] \\ V_{pcc,\alpha}(k) \\ V_{pcc,\beta}(k) \\ V_{load1+,\alpha}(k)cos\Delta\vartheta - V_{load1+,\beta}(k)sin\Delta\vartheta \\ V_{load1+,\alpha}(k)sin\Delta\vartheta + V_{load1+,\beta}(k)cos\Delta\vartheta \\ V_{load1-,\alpha}(k)cos\Delta\vartheta + V_{load1-,\beta}(k)sin\Delta\vartheta \\ -V_{load1-,\alpha}(k)sin\Delta\vartheta + V_{load1-,\beta}(k)cos\Delta\vartheta \\ V_{load5-,\alpha}(k)cos5\Delta\vartheta + V_{load5-,\beta}(k)sin5\Delta\vartheta \\ -V_{load5-,\alpha}(k)sin5\Delta\vartheta + V_{load5-,\beta}(k)cos5\Delta\vartheta \\ V_{load7+,\alpha}(k)cos7\Delta\vartheta - V_{load7+,\beta}(k)sin7\Delta\vartheta \\ V_{load7+,\alpha}(k)sin7\Delta\vartheta + V_{load7+,\beta}(k)cos7\Delta\vartheta \\ R_{load}(k) \\ L_{load}(k) \end{bmatrix}}_{=f(x(k))} \begin{bmatrix} i_{pcc,\alpha}(k) \\ i_{pcc,\beta}(k) \\ V_{pcc,\alpha}(k) \\ V_{pcc,\beta}(k) \\ V_{load1+,\alpha}(k) \\ V_{load1+,\beta}(k) \\ V_{load1-,\alpha}(k) \\ V_{load1-,\beta}(k) \\ V_{load5-,\alpha}(k) \\ V_{load5-,\beta}(k) \\ V_{load7+,\alpha}(k) \\ V_{load7+,\beta}(k) \\ R_{load}(k) \\ L_{load}(k) \end{bmatrix}$$

$$+ \begin{bmatrix} q_{i_{pcc,\alpha}}(k) \\ q_{i_{pcc,\beta}}(k) \\ q_{V_{pcc,\alpha}}(k) \\ q_{V_{pcc,\beta}}(k) \\ q_{V_{load1+,\alpha}}(k) \\ q_{V_{load1+,\beta}}(k) \\ q_{V_{load1-,\alpha}}(k) \\ q_{V_{load1-,\beta}}(k) \\ q_{v_{load5-,\alpha}}(k) \\ q_{V_{load5-,\beta}}(k) \\ q_{V_{load7+,\alpha(k)}} \\ q_{V_{load7+,\beta(k)}} \\ q_{R_{load}}(k) \\ q_{L_{load}}(k) \end{bmatrix} \tag{5.5}$$

$$y(k) = \begin{bmatrix} i_{pcc,\alpha}(k) \\ i_{pcc,\beta}(k) \\ V_{pcc,\alpha}(k) \\ V_{pcc,\beta}(k) \end{bmatrix} = \underbrace{\begin{bmatrix} 1 & 0 & 0 & 0 & 0 & 0 & 0 & 0 & 0 & 0 & 0 & 0 & 0 & 0 \\ 0 & 1 & 0 & 0 & 0 & 0 & 0 & 0 & 0 & 0 & 0 & 0 & 0 & 0 \\ 0 & 0 & 1 & 0 & 0 & 0 & 0 & 0 & 0 & 0 & 0 & 0 & 0 & 0 \\ 0 & 0 & 0 & 1 & 0 & 0 & 0 & 0 & 0 & 0 & 0 & 0 & 0 & 0 \end{bmatrix}}_{=G} \begin{bmatrix} i_{pcc,\alpha}(k) \\ i_{pcc,\beta}(k) \\ V_{pcc,\alpha}(k) \\ V_{pcc,\beta}(k) \\ V_{load,\alpha}(k) \\ V_{load,\beta}(k) \end{bmatrix} + \begin{bmatrix} r_{i_{pcc,\alpha}}(k) \\ r_{i_{pcc,\beta}}(k) \\ r_{V_{pcc,\alpha}}(k) \\ r_{V_{pcc,\beta}}(k) \end{bmatrix} \tag{5.6}$$

Where T_S is the sampling time and $\Delta\vartheta$ is the rotation angle resolution:

$$\Delta\vartheta = 2\pi f_{grid} T_S \tag{5.7}$$

The Matlab script for EKF is shown in appendix ,and the initialized parameters for the EKF is shown in **Tab 5.1.1**:

Parameter	Description	Initialized value
T_S	Sampling time	$5 \times 10^{-5}\mathbf{I}$
f_{grid}	Grid fundamental frequency	$50Hz$
P_0	Initial error covariance matrix	$1 \times 10^{-9}\mathbf{I}$
R	Measurement covariance matrix	$5 \times 10^{-5}\mathbf{I}$
Q_0	Initial input covariance matrix	$1 \times 10^{-9}\mathbf{I}$
x_0	Initial state	$\mathbf{0}$

Table 5.2: Initialized EKF parameters for harmonics estimation

The obtained estimation of the states $V_{load5-,\alpha}, V_{load5-,\beta}, V_{load7+,\alpha}(k), V_{load7+,\beta}$ using AEKF is shown in **Fig 5.7**.

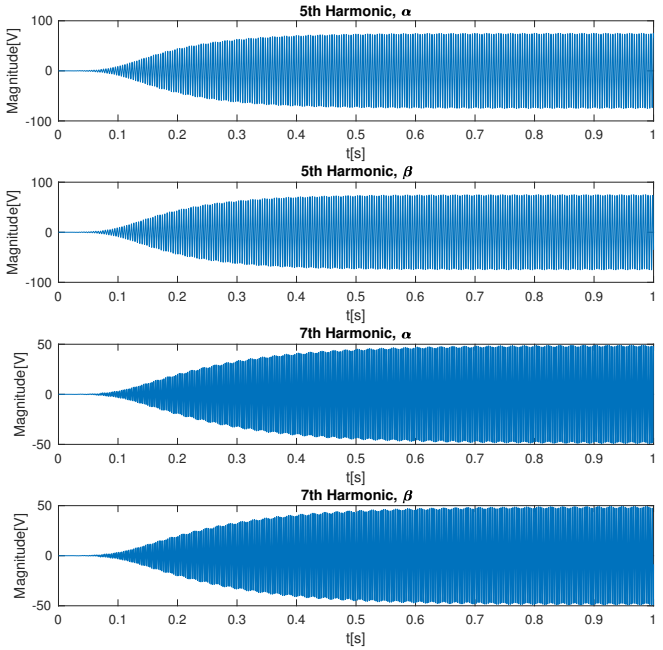

Figure 5.7: The obtained 5th and 7th AC voltage harmonics in $\alpha\beta$ frame by using EKF.

The $\alpha\beta$-phase of the voltage harmonics states is then be used to calculate its amplitude

and phase angle:

$$A_i = \sqrt{V_{loadi,\alpha}^2 + V_{loadi,\beta}^2}$$
$$\phi_i = arctan(\frac{V_{loadi,\alpha}}{V_{loadi,\beta}}) \tag{5.8}$$

Where i is the order of harmonics.

The calculated harmonics amplitude and phase angle is shown in **Fig 5.8**.

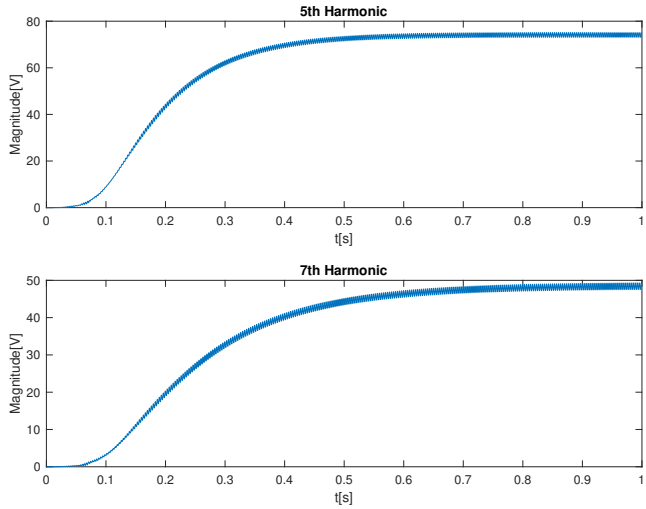

Figure 5.8: The obtained amplitude of 5th and 7th AC voltage harmonics by using EKF. $P_0 = 10^-9$

Discussion

Tuning EKF could be a difficult task. Finding the optimal parameters for the EKF is challenging especially due to the trade-off between speed and accuracy caused by initial error covariance matrix P_0. **Fig 5.9** uses 10^-4 for P_0, and when comparing to **Fig 5.8** it can be observed that value of P_0 makes significant impact on the performance. Lower P_0 gives more accurate value while higher P_0 gives better response time.

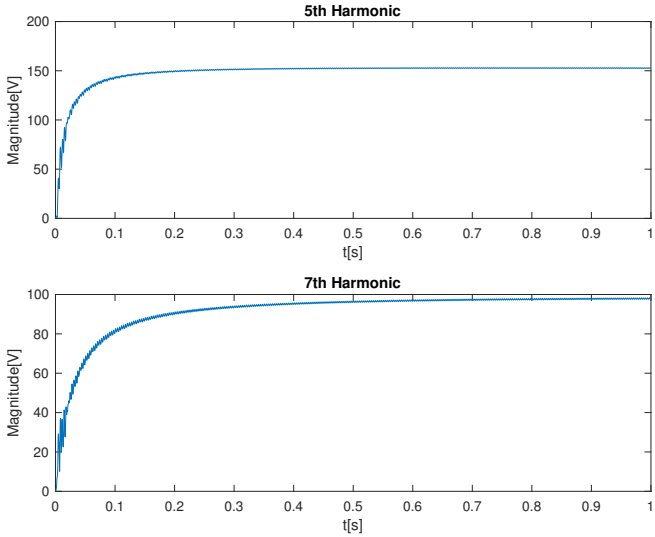

Figure 5.9: The obtained amplitude of 5th and 7th AC voltage harmonics by using EKF. $P_0 = 10^{-4}$

This matter is brought up in [25, p.3]. Observe in **Fig 5.7** that there are significant amount of oscillation in the $\alpha\beta$-phase of the voltage harmonics states. This is an indication of the Q and R being sub-optimal as they are constants through out the estimation process.

One option is to resolve this problem is to find the optimal Q and R using a Genetic Algorithm. But it increases the computational load and complexity. It is much more appealing to resolve this problem by making the input covariance matrix Q adaptive, which is discussed in the next section.

5.1.2 Parameter Estimation based on Adaptive Extended Kalman Filter

Adaptive Extended Kalman Filter(AEKF) is discussed in paper such as Akhlaghi(2017) [26], which uses a forgetting factor $0 \leqslant \alpha \leqslant 1$ to adaptively estimate the covariance matrices. However the forgetting factor α could be tricky to determine.
Our AEKF implementation is detailed in Appendix, and it is inspired by the AKF algorithm by Anders in [11, p.23] and the self tuning algorithm in Jose(2006)[22]. The measurement innovation term $d = y_{k+1} - g_{k+1}\hat{x}^-_{k+1}$ multiplied with the Kalman constant is our basis for estimating the model error $\hat{\omega}$:

$$\hat{\omega_{k+1}} = K_{k+1}(y_{k+1} - g_{k+1}\hat{x}^-_{k+1}) \tag{5.9}$$

Which is used for calculating the estimated model error covariance:

$$\hat{Q_k} = \frac{1}{n}\sum_{i}^{n} \hat{w}^2_{k,i} \cdot I = \hat{q} \cdot I \tag{5.10}$$

Where $\hat{q}$ is the diagonal element of $\hat{Q}$, and n is the number of elements in $\hat{\omega}_k$. To find the optimal $\hat{Q}$, the steps below will be repeated until the stopping criteria is satisfied(j is the covariance update iteration index):

$$P_{k+1}^{j-} = F_k P_k F_k^T + \hat{Q}_k^j \tag{5.11}$$

$$K_{k+1}^j = P_{k+1}^{j-} G_{k+1} (G_{k+1} P_{k+1}^{-} G_{k+1}^T + R_k)^{-1} \tag{5.12}$$

$$\hat{x}_{k+1}^j = \hat{x}_{k+1}^- + K_{k+1}^j (y_{k+1} - g_{k+1}(\hat{x}_{k+1}^-)) \tag{5.13}$$

$$\hat{\omega}_{k+1}^{j+1} = K_{k+1}^j (y_{k+1} - g_{k+1} \hat{x}_{k+1}^j) \tag{5.14}$$

$$\hat{Q_k}^{j+1} = \frac{1}{n} \sum_{i}^{n} (\hat{w}_{k+1,i}^{j+1})^2 \cdot I \tag{5.15}$$

until $|\hat{q}^{j+1} - \hat{q}^j| < \epsilon$ or reached the maximum number of iterations N.

The initialized parameters for the AEKF is shown in **Tab 5.1.2**:

Parameter	Description	Initialized value
T_S	Sampling time	$5 \times 10^{-5}\mathbf{I}$
f_{grid}	Grid fundamental frequency	$50Hz$
P_0	Initial error covariance matrix	$6 \times 10^{-4}\mathbf{I}$
R	Measurement covariance matrix	$1 \times 10^{-5}\mathbf{I}$
Q_0	Initial input covariance matrix	$1 \times 10^{-3}\mathbf{I}$
x_0	Initial state	$\mathbf{0}$
ϵ	Covariance estimation error threshold	1×10^{-8}
N	Maximum iterations for each time-step	10

Table 5.3: Initialized AEKF parameters for harmonics estimation

The obtained estimation of the states $V_{S5-,\alpha}, V_{S5-,\beta}, V_{S7+,\alpha}(k), V_{S7+,\beta}$ using AEKF is shown in **Fig 5.10**

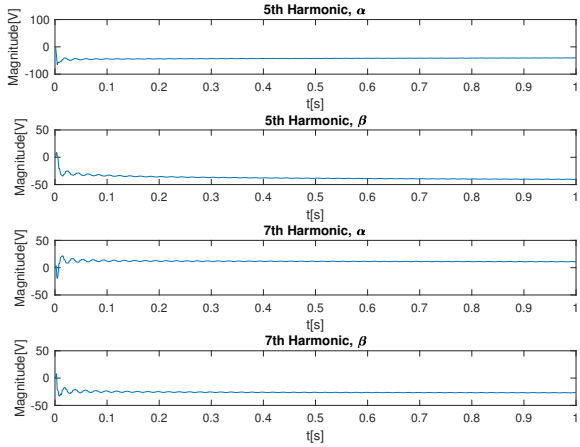

Figure 5.10: The obtained 5th and 7th harmonics in $\alpha\beta$ frame by using AEKF.

The calculated harmonics amplitude and phase angle is shown in **Fig 5.11**.

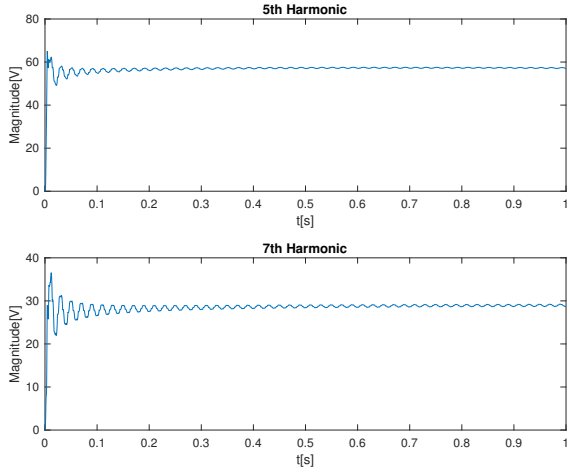

Figure 5.11: The obtained amplitude of 5th and 7th harmonics by using AEKF.

To verify the accuracy of the AEKF, we use the *Sequence Analyzer* block in Simulink.

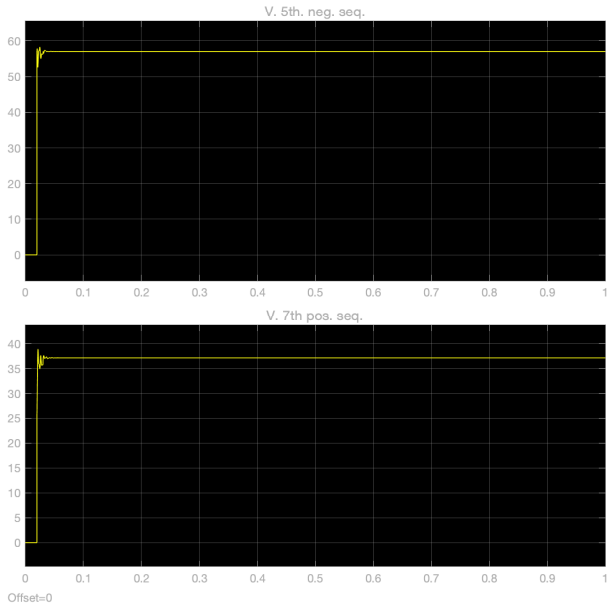

Figure 5.12: The obtained 5th and 7th voltage harmonics amplitude using Sequence Analyzer.

Discussion

Comparing **Fig 5.10** to **Fig 5.8**, the oscillations in $\alpha\beta$ phases are no longer present in the AEKF. The response of AEKF is also much faster, as it reaches the correct state value instantly with some minor oscillation. The trade-off between accuracy and response time are now minimized by utilizing an adaptive input covariance matrix Q. It also greatly simplifies the tuning process. Tuning the two variables P_0 and R is straight forward through trial and error. The effect of each variable on the estimation result is easily detectable and therefore finding the optimal value is much easier.

The Sequence Analyzer indicates that the amplitude of the 5th and 7th voltage harmonic to be respectively 57.05 and 37.12. Reading off from **Fig 5.11** the 5th and 7th voltage harmonic amplitude are estimated to be 57 and 29. AEKF estimates the 5th order harmonic accurately, but the 7th order harmonic is off by an error of 21%. This could be cause by the non-modeled higher order harmonics which is not included in this implementation AEKF. For both EKF and AEKF the state transformation matrix A is not an identity matrix, which means the states are dependent on each other. This raises the possibility of the states accuracy being negatively impacted when higher order harmonics is not included.

Another reason for the performance issues in AEKF and EKF could stem from the fact that EKFs model assumes that the system load is inductive-resistive. Our actual system load also includes capacitive component, which is not taken into consideration. Adding capacitive components to the system model will add more complexity to the system model. The usage of jacobian for the calculation of the linearized transfer function may be a minor factor in the performance issues and contribute to deviance in the results.

5.1.3 Parameter Estimation based on Adaptive Kalman Filter

Another alternative for estimating the input impedance for the load subsystem by using the Adaptive Kalman Filter(AFK) algorithm, which is described in section 3.11. It differs from the EKF in that it utilizes a Random Walk model for the states transformation instead of the non-linear state transformation. This means that the state transformation matrix A is an identity matrix. For AKF the system is formulated in state-space form by applying Fortescue Theorem(**Ch 3.8.1**) and Clarke Transformation(**Ch 3.8.2**) on the three-phase signal:

$$\begin{aligned} V_a(t) &= A_a(t)cos(\omega(t)t + \phi_a(t)) \\ V_b(t) &= A_a(t)cos(\omega(t)t + \phi_a(t) - \frac{2\pi}{3}) \\ V_c(t) &= A_a(t)cos(\omega(t)t + \phi_a(t) + \frac{2\pi}{3}) \end{aligned} \tag{5.16}$$

, one would obtain:

$$\begin{aligned} \begin{bmatrix} V_\alpha(t) \\ V_\beta(t) \end{bmatrix} &= \sum_{i \in h_p} \begin{bmatrix} cos(i\omega(t)) & -sin(i\omega(t)) \\ sin(i\omega(t)) & cos(i\omega(t))) \end{bmatrix} \begin{bmatrix} A_{i,p}cos(\phi_{i,p}) \\ A_{i,p}sin(\phi_{i,p}) \end{bmatrix} \\ &+ \sum_{i \in h_n} \begin{bmatrix} cos(i\omega(t)) & -sin(i\omega(t)) \\ -sin(i\omega(t)) & -cos(i\omega(t))) \end{bmatrix} \begin{bmatrix} A_{i,n}cos(\phi_{i,n}) \\ A_{i,n}sin(\phi_{i,n}) \end{bmatrix} \end{aligned} \tag{5.17}$$

By writing $A_i cos(\phi_i)$ and $A_i sin(\phi_i)$ as the system states $x_{i,1}$ and $x_{i,2}$, and also writing $V_\alpha(t)$ and $V_\beta(t)$ as the system measurement y, we obtain the system state-space model for our AKF in discrete time[27, p.2] k:

$$y[k] = \sum_{i \in h_p} \begin{bmatrix} cos(i\omega\Delta tk) & -sin(i\omega\Delta tk) \\ sin(i\omega\Delta tk) & cos(i\omega\Delta tk) \end{bmatrix} \begin{bmatrix} x_{i,1} \\ x_{i,2} \end{bmatrix}_k$$

$$+ \sum_{i \in h_n} \begin{bmatrix} cos(i\omega\Delta tk) & -sin(i\omega\Delta tk) \\ -sin(i\omega\Delta tk) & -cos(i\omega\Delta tk) \end{bmatrix} \begin{bmatrix} x_{i,1} \\ x_{i,2} \end{bmatrix}_k \tag{5.18}$$

$$\begin{bmatrix} x_{i,1} \\ x_{i,2} \end{bmatrix}_{k+1} = \begin{bmatrix} 1 & 0 \\ 0 & 1 \end{bmatrix} \begin{bmatrix} x_{i,1} \\ x_{i,2} \end{bmatrix}_k \tag{5.19}$$

Where the three phase synthetic signal is measured at the three phase PCC close to the diode bridge(as seen in **Fig A.1**). It is then transformed into $\alpha\beta$ frame using Clarke transformation (**Ch 3.8.2**) and fed into the AKF as the measured state $y[k]$. The AKF is then able to compute and estimate the state $\hat{X}$, which can be used to extract the magnitude and phase angle of the *ith* harmonic:

$$\begin{aligned} A_i &= \sqrt{x_{i,1}^2 + x_{i,2}^2} \\ \phi_i &= arctan(\frac{x_{i,2}}{x_{i,1}}) \end{aligned} \tag{5.20}$$

The *ith* harmonics can also be expressed in polar form and its angel representation:

$$X_i = A_i e^{j\phi_i} = A_i \angle \phi_i \tag{5.21}$$

The Matlab script and for the AKF initialization is shown in **Appendix B.3**.
The initialized AKF parameters for the voltage signal is shown in **Tab 5.1.3**. The tuning process is straight forward with R and P being the main factor for the performance. Trough trial and error it is observed that decreasing R will lead to less oscillation in the stabilized states, but allowing more "spikes" in the initial transient period. While decreasing P cause

the states to stabilize faster.

Parameter	Description	Initialized value
T_S	Sampling time	$5 \times 10^{-5}\mathbf{I}$
f_{grid}	Grid fundamental frequency	$50Hz$
H_p	Set of positive sequence harmonics	$[1, 7, 13]$
H_n	Set of negative sequence harmonics	$[1, 5, 11]$
P_0	Initial error covariance matrix	$1 \times 10^{-3}\mathbf{I}$
R	Measurement covariance matrix	$1 \times 10^{-9}\mathbf{I}$
Q_0	Initial input covariance matrix	$\mathbf{0}$
x_0	Initial state	$\mathbf{0}$
ϵ	Covariance estimation error threshold	1×10^{-9}
N	Maximum iterations for each time-step	10

Table 5.4: Initialized AKF parameters for harmonics estimation in grid voltage signal

The result of the voltage harmonics eatimation matches very well with the Sequence Analysis in **Fig 5.14**. Values obtained through both methods deviates only around 0.2, which indicates a correct AKF model. The AKF is responsive, as the states stabilizes after 0.04 seconds. The estimated harmonics phase angle also coincides well with the Sequence Analyzer, with a deviance of $\leqslant 0.02$. Observe that there is a periodic spikes in the 13th harmonics phase estimation that swings between $-\pi$ and π. This is because the phase angle is calculated by *Four-quadrant inverse tangent function*. In cases where $x_{i,2}$ is negative and $x_{i,1}$ fluctuates between positive and negative values, the phase angle will also fluctuated between the second and third quadrant.

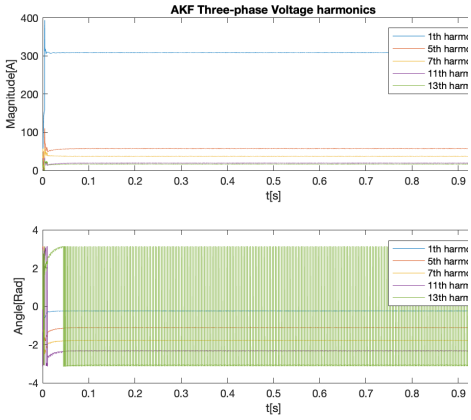

(a) The obtained amplitude and phase angle of 5th, 7th, 11th and 13th voltage harmonics using AKF

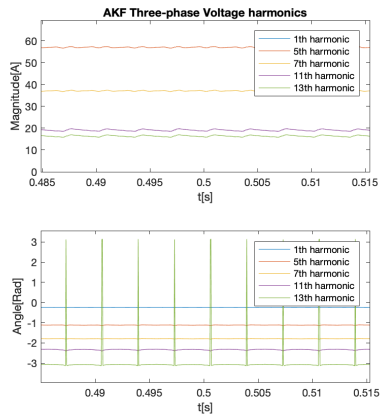

(b) Zoomed in around 0.5s

Figure 5.13: AKF voltage harmonics estimation

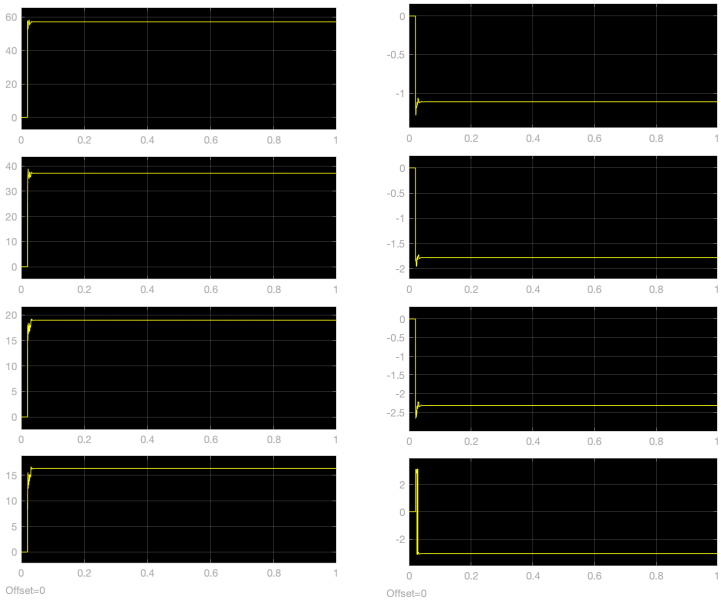

(a) The obtained 5th, 7th, 11th and 13th voltage harmonics amplitude using Sequence Analyzer.

(b) The obtained 5th, 7th, 11th and 13th voltage harmonics phase using Sequence Analyzer.

Figure 5.14: Sequence Analysis of the PCC voltage

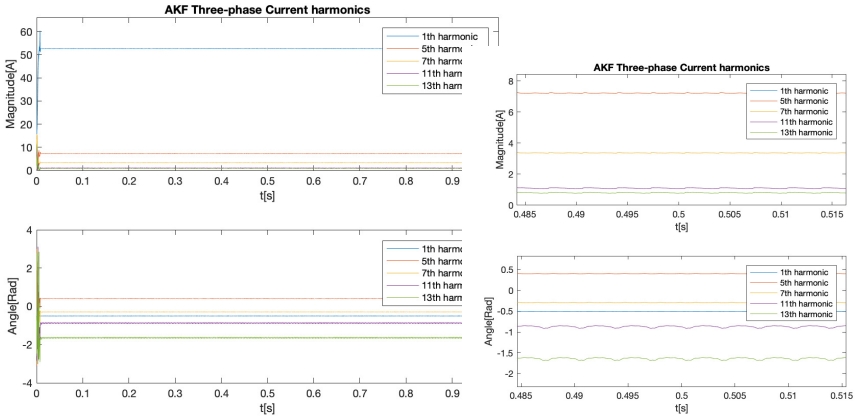

(a) The obtained amplitude and phase angle of 5th, 7th, 11th and 13th current harmonics using AKF

(b) Zoomed in around 0.5s

Figure 5.15: AKF current harmonics estimation

Next we perform AKF on the three phase PCC current. The initialized parameters for the AKF is shown below. The estimated current harmonics are displayed in **5.15**.

Parameter	Description	Initialized value
T_S	Sampling time	$5 \times 10^{-5}\mathbf{I}$
f_{grid}	Grid fundamental frequency	$50Hz$
H_p	Set of positive sequence harmonics	$[1, 7, 13]$
H_n	Set of negative sequence harmonics	$[1, 5, 11]$
P_0	Initial error covariance matrix	$1 \times 10^{-5}\mathbf{I}$
R	Measurement covariance matrix	$1 \times 10^{-10}\mathbf{I}$
Q_0	Initial input covariance matrix	$\mathbf{0}$
x_0	Initial state	$\mathbf{0}$
ϵ	Covariance estimation error threshold	1×10^{-9}
N	Maximum iterations for each time-step	10

Table 5.5: Initialized AKF parameters for harmonics estimation in grid current signal

After obtaining the magnitude and phase of 5th, 7th 11th and 13th order harmonics in both voltage and current, we can now calculate the harmonics impedance through complex division:

$$Z_{ith} = \frac{V_{ith}\angle\Phi_{ith}}{I_{ith}\angle\phi_{ith}} = \frac{V_{ith}}{I_{ith}}\angle(\Phi_{ith} - \phi_{ith}) \tag{5.22}$$

The estimated harmonics impedance is shown in **Tab 5.6**

Harmonics Order	Voltage(V)	Current(A)	Impedance(Ω)
1(positive)	$309.19\angle -0.24$	$52.68\angle -0.48$	$5.87\angle 0.24$
5	$57.08\angle -1.11$	$7.22\angle 0.48$	$7.9\angle -1.59$
7	$37.13\angle -1.79$	$3.37\angle -0.18$	$11.03\angle -1.61$
11	$19.14\angle -2.33$	$1.10\angle -0.71$	$17.33\angle -1.62$
13	$16.42\angle -3.06$	$0.81\angle -1.45$	$20.37\angle -1.61$

Table 5.6: AKF harmonics impedance estimation

Discussion

This AKF differs from previous EKFs methods in that it utilizes a random-walk model for the state transformation matrix, meaning that the A matrix is an identity matrix(**Eq 5.19**). The states are therefore modeled as being independent from each other. The AKF has proven give much better estimation than the AEKF, which indicates that AKF models the system more accurately.

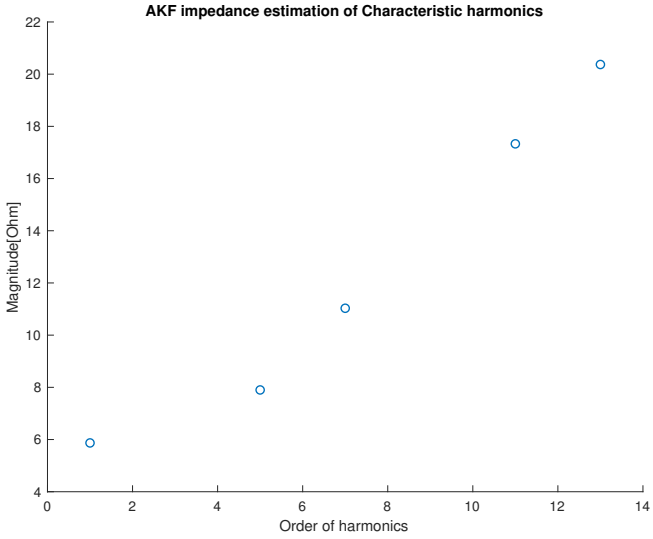

Figure 5.16: Plot of characteristic harmonics impedance.

Fig 5.16 shows the obtained harmonics impedance amplitude plotted against the harmonics order. Observe that the amount of points are scarce, which is caused by the nature of the characteristic harmonics($6k \pm 1$). The impedance information in between them are unknown and could lead to incorrect evaluation of the system dynamic. We wish to explore the possibilities of gaining more information of the non-characteristic harmonics. One possibility is to use the impedance mapping method from Bing(2009)[7], which is discussed in the next section.

5.2 Use the DC Side PCC As the Operation Point

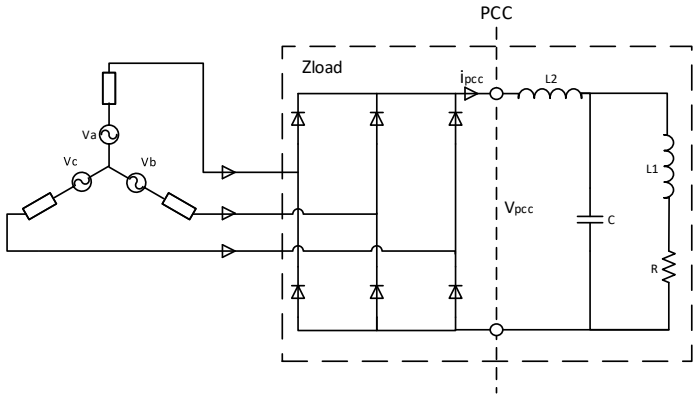

Figure 5.17: Equivalent system impedance model with the operation point at the DC side.

Here the operation point is set at the DC side close to the diode bridge. The DC load impedance Z_{dc} can be found by either using complex division between v_{pcc} and i_{pcc}, or the analytic model of the load components.

$Z_{dc}(\omega)$ is the analytic expression of DC impedance of angular frequency ω. For our system where there is a inductor L_2 in series with a parallel of a capacitor C and a series of inductor L_1 and resistor R, it is expressed as:

$$Z_{dc}(\omega) = \omega L_2 + \frac{1}{\omega C + \dfrac{1}{R + \omega L_1}} \tag{5.23}$$

5.2.1 Harmonics Linearization Mapping Method

The input impedance of the load subsystem Z_{load} could also be modeled using the concept *Harmonics Linearization*, which is introduced in Sun(2008)[28] and further generalizes in Sun(2009)[29]. It utilizes analytical mapping functions S that describe voltage and current transfer through general multi-pulse rectifiers, such that the load input impedance can be expressed as a function of the DC impedance Z_{dc} as shown in **Fig 5.17**. The harmonic linearization specifically for three-phase six-pulse rectifiers is detailed in Bing(2009)[7]. This method assumes that the DC current is continuous, and that the diodes are ideal.

The Positive-sequence load input impedance is expressed as:

$$\begin{aligned} Z_{load-p}(s) = \frac{\pi^2}{9}\Bigg\{ \sum_{m=-\infty}^{\infty} \Bigg[& \frac{1}{(1-36m^2)} \frac{1}{Z_{dc}(j12\pi m f_{nom})} \\ & + \frac{1}{(1-6m^2)} \frac{1}{Z_{dc}(s + j2\pi(6m-1)f_{nom})} \Bigg] \Bigg\}^{-1} \end{aligned} \tag{5.24}$$

The Negative-sequence load input impedance is expressed as:

$$Z_{load-n}(s) = \frac{\pi^2}{9}\left\{ \sum_{m=-\infty}^{\infty} \left[\frac{1}{(1-36m^2)} \frac{1}{Z_{dc}(j12\pi m f_{nom})} + \frac{1}{(1+6m^2)} \frac{1}{Z_{dc}(s+j2\pi(6m+1)f_{nom})} \right] \right\}^{-1} \tag{5.25}$$

The calculated AC impedance using **Eq 5.24** and **Eq 5.25** are shown in **Fig 5.18** and **Fig 5.6**, where the system components are initialized as in **Tab 5.1**. The Matlab code for calculating the AC impedance is shown in **Appendix B.4**.

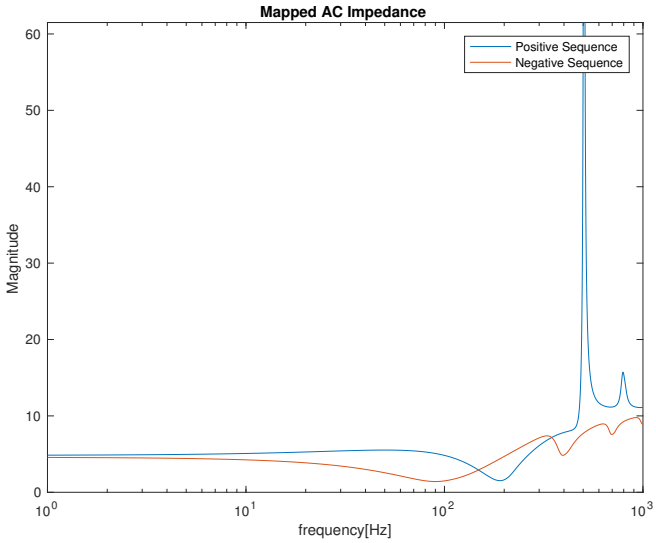

Figure 5.18: Mapped load input impedance using harmonics linearization.

Harmonics Order	Impedance Magnitude(Ω)
1th	5.53
5th	6.09
7th	7.22
11th	8.44
13th	11.22

Table 5.7: Load input impedance harmonics magnitude

5.2.2 Discussion

Harmonics linearization method is able to map the impedance of an entire frequency range and thus provides more information on the system impedance than AKF. Being able to

analyze the system impedance over a large frequency range will bring valueble insight into the system stability and behavior. However, comparing the harmonics impedance obtained through AKF in **Tab 5.6** and harmonics linearizaiton modeling in **Tab 5.7**, it shows higher discrepancies for higher order of harmonics. The author would argue that this is caused by the inaccuracy of the harmonics linearization for higher frequencies. The harmonics linearization method is based on so a called *Small signal method*, which assumes small variation in the voltage and current.

In comparison AKF is a much more accurate method of system impedance estimation. By directly measuring at the PCC and extracting the harmonics from the signal measurement, the AKF is also more robust against disturbances and discrepancies. We will explore another possibility of gaining more information on the non-characteristic impedance using the AKF and signal injection, which is discussed in the next chapter.

Chapter 6

Transient analysis

In this chapter the transient response of the system will be analyzed.

The system will be injected with a step function in order to analyze its step response. **Appendix A.2** shows the Simulink implementation of the voltage step injection. It is done with a series connected *Controlled Voltage Source* block on the load bus. The input of the *Controlled Voltage Source* is a step function of 100 in magnitude and step time $t = 0.5$.

6.1 Expanded AKF

In order to extract the impedance of more frequencies, we expand the states of AKF to include non-characteristic harmonics.

Parameter	Description	Initialized value
T_S	Sampling time	$5 \times 10^{-5}\mathbf{I}$
f_{grid}	Grid fundamental frequency	$50Hz$
H_p	Set of positive sequence harmonics	$[1, 2, 3, 4, 5, 6, \cdots, 20]$
H_n	Set of negative sequence harmonics	$[1, 2, 3, 4, 5, 6, \cdots, 20]$
P_0	Initial error covariance matrix	$1 \times 10^{-2}\mathbf{I}$
R	Measurement covariance matrix	$1 \times 10^{1}\mathbf{I}$
Q_0	Initial input covariance matrix	$\mathbf{0}$
x_0	Initial state	$\mathbf{0}$
ϵ	Covariance estimation error threshold	1×10^{-9}
N	Maximum iterations for each time-step	10

Table 6.1: Initialized Expanded AKF parameters for harmonics estimation in grid voltage signal

The AKF is now configured to estimate both the positive and negative sequence for up to the 20th harmonic.

To verify the its accuracy, we apply the expanded AKF to our orignal grid voltage signal without the perturbation.

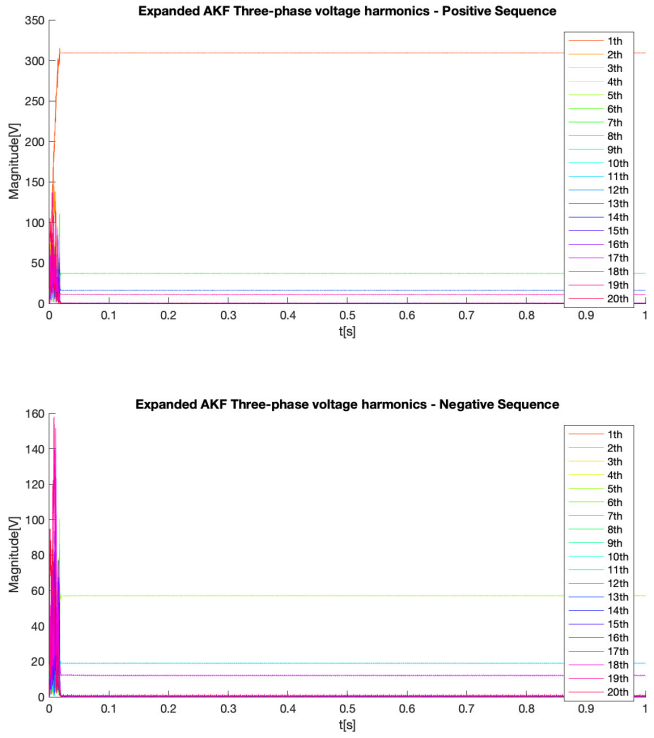

Figure 6.1: Estimated voltage harmonics with the expanded states.

As expected, we observe the steady state value of 1th, 7th, 13th, 19th harmonics in the positive sequence and 5th, 11th 17th harmonics in the negative sequence, with the rest being zero. The value of these characteristic harmonics also have the same value as we have obtained before, which further confirms its accuracy.

6.2 Step Function

A step function is also known as *Heaviside step function*. It can be defines as a piecewise constant function:

$$f(x) = \begin{cases} 0 & \text{if x} < t \\ \frac{1}{2} & \text{if x} = t \\ 1 & \text{if x} > t \end{cases}$$

Where t is the step time.

This will induce a controlled perturbation to the system.

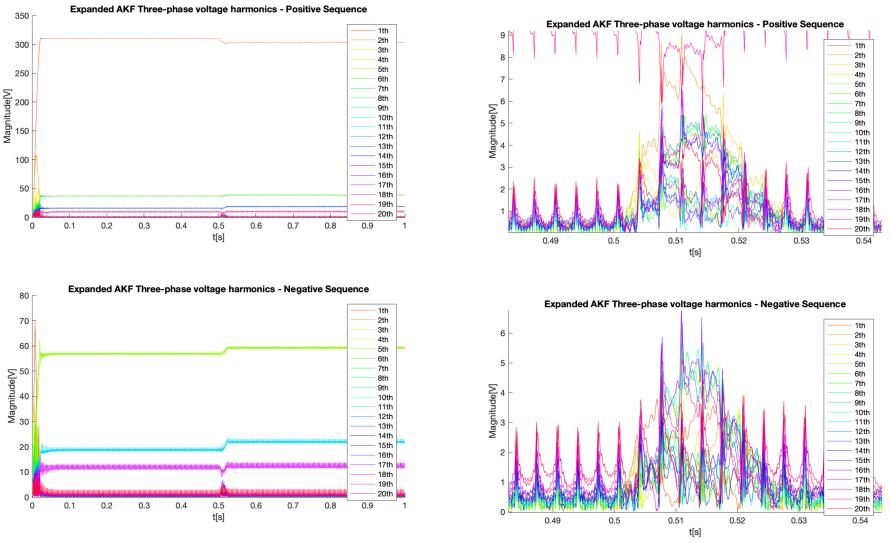

(a) Obtained voltage harmonics with the signal injection

(b) Zoomed in around 0.52 s

Figure 6.2: Expanded AKF of voltage harmonics estimation

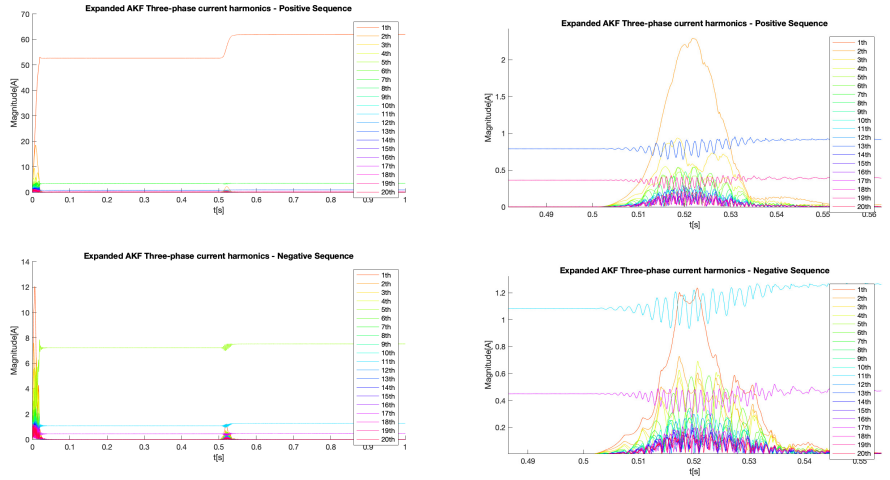

(a) Obtained current harmonics with the signal injection

(b) Zoomed in around 0.52 s

Figure 6.3: Expanded AKF of current harmonics estimation

6.3 Perturbed System Estimation result

The estimation results are shown in **Fig 6.2** and **Fig 6.3**. Observe that the steady state(in voltage and current) of the characteristic harmonics alters after the signal injection. The calculated impedance of the 1th harmonic(fundamental frequency) is decreased due to the injection, while the impedance of the rest of the characteristic harmonics(5th, 7th, 11th, 13th, 17th, 19th) remains the same.

During the transient period between 0.5 and 0.54 seconds, there is also induced responses of the non-characteristic harmonics. We will look into the possibility of extracting harmonics impedance using these signals.

6.4 Harmonics Impedance Extraction

For the characteristic harmonics we can extract its impedance by simply dividing the steady state voltage with the steady state current. For non-characteristic harmonics however, the signal responses are not in steady states and are varying with time. To resolve this time dependency problem, we will extract the harmonics impedance using an average method. A similar impedance extraction using average mathematical model is discussed in Khan(2018)[30]. We will use the average values of the entire transient period to calculate the respective impedance of the harmonics.

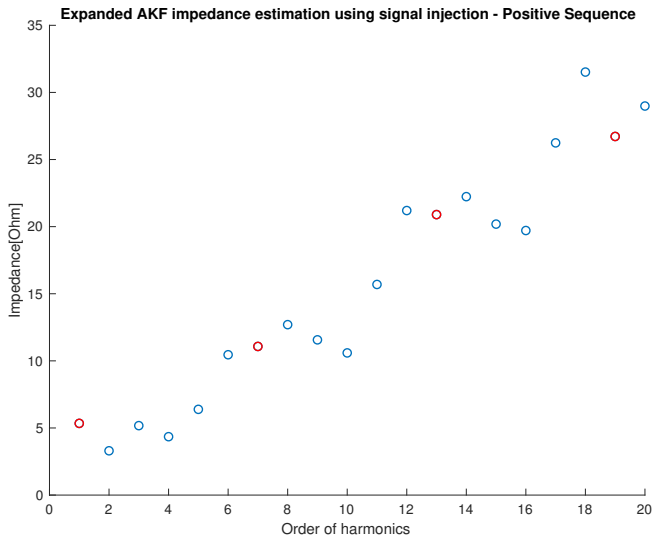

Figure 6.4: Calculated impedance of the positive sequence using average method. Characteristic harmonics are marked in red.

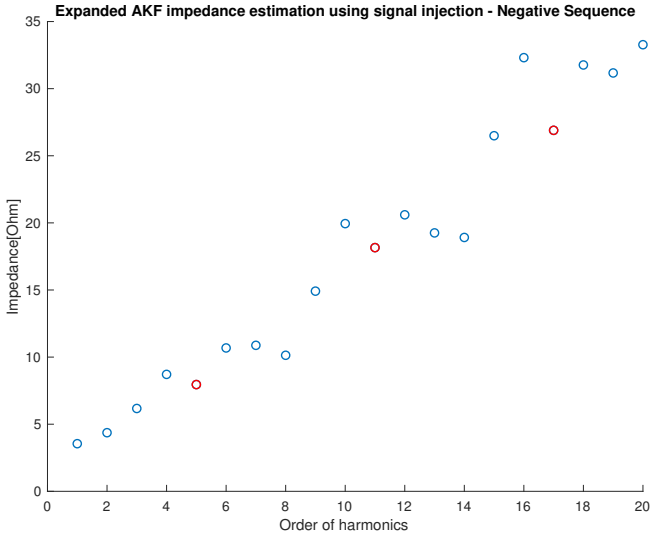

Figure 6.5: Calculated impedance of the negative sequence using average method. Characteristic harmonics are marked in red.

6.5 Discussion

Both **Fig 6.4** and **Fig 6.5** shows an upward trend of the impedance with the increase of harmonics order. The impedance of the characteristic harmonics(marked in red circle) fit in well with the non-characteristic harmonics. The points are approximately linear in structure and resembles a cyclic pattern in a period of 6 points, which corresponds with the 6-pulse of the rectifier.

Outliers in the plots seems to be correlated. In **Fig 6.4**, the positive sequence harmonics of order 4, 10 and 16 have much lower magnitude than the linear structure of the plot. In **Fig 6.5**, the negative sequence harmonics of order 4, 10 and 16 have higher magnitude than the linear structure of the plot.

This type of step change injection on the load bus resembles a load change. This gives way for analyzing the transient caused by load side changes instead of forced injection, given that one is able to isolated the event from rest of the grid activities.

The injected voltage in our case has a magnitude of 100, which is a relatively high perturbation value compared to the nominal DC voltage V_{dc} for our system which is around 500V. Smaller perturbation magnitude will impact the estimation accuracy especially for higher order harmonics as the transient response become to small to estimate precisely.

Observe in **Fig 6.3b** and **Fig 6.2b** that higher order harmonics has significantly lower readings. Estimation of harmonics with order higher than 20 will be significantly distorted due to their lower amplitude.

Chapter 7

Conclusion and Future Work

In this master's thesis, several parameter identification methods that aims to estimate the harmonics impedance are proposed and verified with the sequence analyzer. A further transient analysis is done by a load side signal injection.

First, three Kalman filter based on-line identification methods are implemented. These methods are tested on a three-phase rectifier system. All three methods shows varying degree of accuracy and responsiveness. The methods with adaptive error covariance holds better performance, while the AKF performed the best overall. It became apparent that the the impedance information provided by the naturally embedded characteristic harmonics is not sufficient for the system impedance assessment. Therefor an impedance mapping method based on harmonics linearizaiton was also implemented to mapped out the impedance of an entire frequency band, but it lacked accuracy for higher order of harmonics.

For further assessment of non-characteristic harmonics impedance, we performed a transient analysis of the load-side signal injected system. We used the expanded AKF to estimated the parameters and calculated the impedance using average method, which shows promising results.

Some problems and possibilities are still left unexplored, and could provide some interesting topics for future papers and master's thesis:

- This experiment has been conducted in a noise-free environment. The on-line identification methods could be further tested with noise and distortions.
- The impedance models and estimated impedance are presented, but the actual stability analysis was not performed in this thesis. Future papers is encourages to calculate the system impedance based on the Nyquist stability criterion.
- The transient analysis was based on a load side signal injection. The author suggests further exploration of potentially using actual load-change induced transients

to calculate harmonics impedance.

Bibliography

[1] Ned Mohan and Tore M Undeland. *Power electronics: converters, applications, and design*. John wiley & sons, 2007.

[2] Patrick Y.C. Hwang Robert Glover Brown. *Introduction to Random Signal and Applied Kalman Filtering*. Wiley, 4 edition, 2012.

[3] Joseph S Subjak and John S Mcquilkin. Harmonics-causes, effects, measurements, and analysis: an update. *IEEE transactions on industry applications*, 26(6):1034–1042, 1990.

[4] Jian Sun. Impedance-based stability criterion for grid-connected inverters. *IEEE Transactions on Power Electronics*, 26(11):3075–3078, 2011.

[5] Hussein A Kazem. Harmonic mitigation techniques applied to power distribution networks. *Advances in power electronics*, 2013, 2013.

[6] Qin Lei, Miaosen Shen, Vlado Blasko, and Fang Z Peng. A generalized input impedance model of three phase diode rectifier. In *2013 Twenty-Eighth Annual IEEE Applied Power Electronics Conference and Exposition (APEC)*, pages 2655–2661. IEEE, 2013.

[7] Zhonghui Bing, Kamiar J Karimi, and Jian Sun. Input impedance modeling and analysis of line-commutated rectifiers. *IEEE Transactions on Power Electronics*, 24 (10):2338–2346, 2009.

[8] Nils Hoffmann and Friedrich Wilhelm Fuchs. Minimal invasive equivalent grid impedance estimation in inductive–resistive power networks using extended kalman filter. *IEEE Transactions on Power Electronics*, 29(2):631–641, 2014.

[9] Haakon Jondal Helle. Methods for identification of instantaneous frequencies for application in isolated microgrid. Master's thesis, NTNU, 2017.

[10] Santiago Sanchez and Marta Molinas. Large signal stability analysis at the common coupling point of a dc microgrid: A grid impedance estimation approach based on a recursive method. *IEEE Transactions on energy conversion*, 30(1):122–131, 2015.

[11] Anders Kjeka Broen. Real-time harmonics tracking for stability assessment of a microgrid. Master's thesis, NTNU, The address of the publisher, 2016.

[12] Mark Sumner, Ben Palethorpe, David WP Thomas, Pericle Zanchetta, and Maria Carmela Di Piazza. A technique for power supply harmonic impedance estimation using a controlled voltage disturbance. *IEEE Transactions on Power Electronics*, 17(2):207–215, 2002.

[13] Lucian Asiminoaei, Remus Teodorescu, Frede Blaabjerg, and Uffe Borup. A new method of on-line grid impedance estimation for pv inverter. In *Nineteenth Annual IEEE Applied Power Electronics Conference and Exposition, 2004. APEC'04.*, volume 3, pages 1527–1533. IEEE, 2004.

[14] Mohammad Amin, Chen Zhang, Atle Rygg, Marta Molinas, Eneko Unamuno, and Mohamed Belkhayat. Nyquist stability criterion and its application to power electronics systems. *Wiley Encyclopedia of Electrical and Electronics Engineering*, pages 1–22, 2019.

[15] A Griffo, J Wang, and D Howe. Large signal stability analysis of dc power systems with constant power loads. In *2008 IEEE Vehicle Power and Propulsion Conference*, pages 1–6. IEEE, 2008.

[16] Jos Arrillaga and Neville R Watson. *Power system harmonics*. John Wiley & Sons, 2004.

[17] Emmanuel Hernández Mayoral, Miguel Angel Hernández López, Edwin Román Hernández, Hugo Jorge Cortina Marrero, José Rafael Dorrego Portela, and Victor Ivan Moreno Oliva. Fourier analysis for harmonic signals in electrical power systems. In *Fourier Transforms-High-tech Application and Current Trends*. InTech, 2017.

[18] IEC Standard. 61000-4-7. *General guide on harmonics and interharmonics measurements for power supply systems and equipment connected thereto*, 2002.

[19] Howard Percy Robertson. The uncertainty principle. *Physical Review*, 34(1):163, 1929.

[20] M. Molinas. Ttk7 adaptive data analysis. 2018.

[21] Rolf Isermann and Marco Münchhof. *Identification of dynamic systems: an introduction with applications*. Springer Science & Business Media, 2010.

[22] J. Macías and A. Gomez Expósito. Self-tuning of kalman filters for harmonic computation. *IEEE TRANSACTIONS ON POWER DELIVERY*, 21(1), 2006. URL `https://ieeexplore.ieee.org/stamp/stamp.jsp?arnumber=1564238`.

[23] C Desoer and Yung-Terng Wang. On the generalized nyquist stability criterion. *IEEE Transactions on Automatic Control*, 25(2):187–196, 1980.

[24] Jens G Balchen, Trond Andresen, and Bjarne A Foss. *Reguleringsteknikk*. NTNU, Institutt for teknisk kybernetikk, 2004.

[25] Karren Kennedy, Gordon Lightbody, and Robert Yacamini. Power system harmonic analysis using the kalman filter. In *2003 IEEE Power Engineering Society General Meeting (IEEE Cat. No. 03CH37491)*, volume 2, pages 752–757. IEEE, 2003.

[26] Shahrokh Akhlaghi, Ning Zhou, and Zhenyu Huang. Adaptive adjustment of noise covariance in kalman filter for dynamic state estimation. In *2017 IEEE Power & Energy Society General Meeting*, pages 1–5. IEEE, 2017.

[27] A.K. Broen, M. Amin, E. Skjong, and M. Molinas. Instantaneous frequency tracking of harmonic distortions for grid impedance identification based on kalman filtering. 2016. doi: 10.1109/COMPEL.2016.7556708. URL `https://ieeexplore.ieee.org/document/7556708`.

[28] Jian Sun and Kamiar J Karimi. Small-signal input impedance modeling of line-frequency rectifiers. *IEEE Transactions on Aerospace and Electronic Systems*, 44 (4):1489–1497, 2008.

[29] Jian Sun, Zhonghui Bing, and Kamiar J Karimi. Input impedance modeling of multi-pulse rectifiers by harmonic linearization. *IEEE Transactions on Power Electronics*, 24(12):2812–2820, 2009.

[30] Shahbaz Khan, Xiaobin Zhang, Bakht Khan, Husan Ali, Haider Zaman, and Muhammad Saad. Ac and dc impedance extraction for 3-phase and 9-phase diode rectifiers utilizing improved average mathematical models. *Energies*, 11(3):550, 2018.

Appendices

Appendix A

Matlab Simulink models

A.1 Three phase diode rectifier model

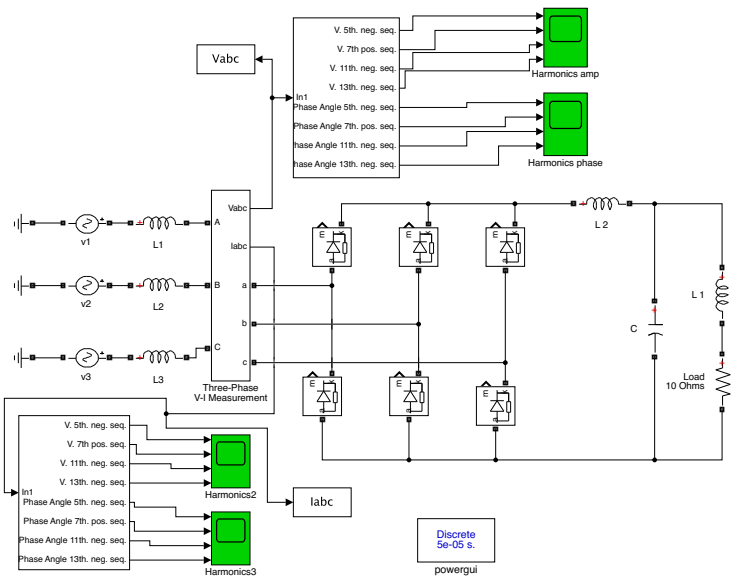

Figure A.1: The three-phase diode rectifier model

A.2 Step function injection

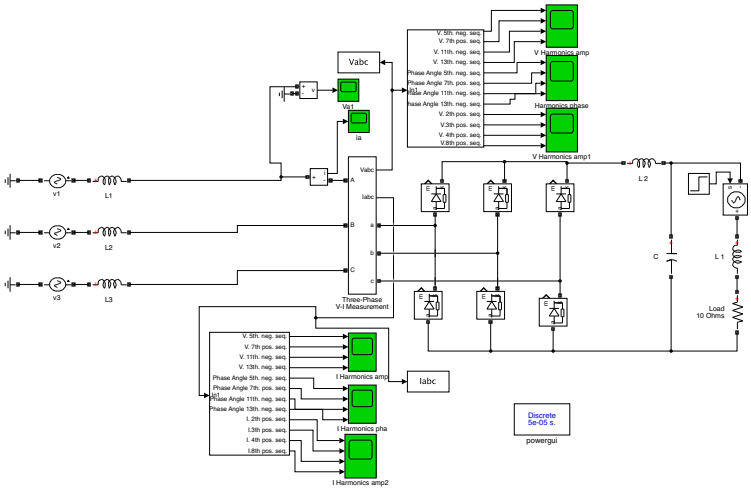

Figure A.2: The simulink model of the series injection of a voltage step on the load bus.

Appendix B

Matlab Code

B.1 Extended Kalman Filter Matlab Function implementation

By Yi Cao at Cranfield University, 02/01/2008

```
function [x,P]=ekf(fstate,x,P,hmeas,z,Q,R)
% EKF   Extended Kalman Filter for nonlinear dynamic systems
% [x, P] = ekf(f,x,P,h,z,Q,R) returns state estimate, x and state ...
    covariance, P
% for nonlinear dynamic system:
%           x_k+1 = f(x_k) + w_k
%           z_k   = h(x_k) + v_k
% where w ¬ N(0,Q) meaning w is gaussian noise with covariance Q
%       v ¬ N(0,R) meaning v is gaussian noise with covariance R
% Inputs:   f: function handle for f(x)
%           x: "a priori" state estimate
%           P: "a priori" estimated state covariance
%           h: fanction handle for h(x)
%           z: current measurement
%           Q: process noise covariance
%           R: measurement noise covariance
% Output:   x: "a posteriori" state estimate
%           P: "a posteriori" state covariance


    [x1,A]=jaccsd(fstate,x);    %nonlinear update and linearization ...
        at current state
    P=A*P*A'+Q;                 %partial update
    [z1,H]=jaccsd(hmeas,x1);    %nonlinear measurement and ...
        linearization
    P12=P*H';                   %cross covariance
    % K=P12*inv(H*P12+R);       %Kalman filter gain
    % x=x1+K*(z-z1);            %state estimate
    % P=P-K*P12';               %state covariance matrix
```

```
27      R=chol(H*P12+R);            %Cholesky factorization
28      U=P12/R;                    %K=U/R'; Faster because of back ...
            substitution
29      x=x1+U*(R'\(z-H*x1));       %Back substitution to get state update
30      P=P-U*U';                   %Covariance update, ...
            U*U'=P12/R/R'*P12'=K*P12.
31  end
32
33  function [z,A]=jaccsd(fun,x)
34  % JACCSD Jacobian through complex step differentiation
35  % [z J] = jaccsd(f,x)
36  % z = f(x)
37  % J = f'(x)
38  %
39      z=fun(x);
40      n=numel(x);
41      m=numel(z);
42      A=zeros(m,n);
43      h=n*eps;
44      for k=1:n
45          x1=x;
46          x1(k)=x1(k)+h*i;
47           A(:,k)=imag(fun(x1))/h;
48      end
49  end
```

B.2 Adaptive Extended Kalman Filter Matlab Function implementation

```
1   function [x,P,Q]=Aekf(fstate,eps_adaptive, ...
        N_iterations,x,P,hmeas,z,Q,R)
2       q_last=Q(1,1);
3       [x1,A]=jaccsd(fstate,x);
4       [z1,C]=jaccsd(hmeas,x1);
5       iter = 0;
6       while iter < N_iterations
7            P_adaptive_ = A*P*A'+ Q;
8            K = P_adaptive_*C'*(C*P_adaptive_*C' + R)^(-1);
9            w_adaptive = K*(z-C*x);
10           x =x+K*(z-C*x);
11           q = 1/length(w_adaptive)*sum(w_adaptive.^2);
12
13           if(abs(q-q_last)<eps_adaptive)
14               break
15           end
16          Q = q*eye(size(Q,1));
17          q_last = q;
18          iter = iter+1;
19      end
20      P = (eye(size(Q,1)) - K*C)*P_adaptive_;
21  end
22
```

```
function [z,A]=jaccsd(fun,x)
% JACCSD Jacobian through complex step differentiation
% [z J] = jaccsd(f,x)
% z = f(x)
% J = f'(x)
%
     z=fun(x);
     n=numel(x);
     m=numel(z);
     A=zeros(m,n);
     h=n*eps;
     for k=1:n
         x1=x;
         x1(k)=x1(k)+h*i;
          A(:,k)=imag(fun(x1))/h;
     end
end
```

B.3 Adaptive Kalman Filter Matlab Initialization Function

```
function [ init_kalman ] = three_adaptive_kalman_struct( hp, hn, ...
    Q0, R, P, x0 )
%ADAPTIV_KALMAN_STRUCT Creates a struct necessary for the adaptive ...
    kalman
%simulink block for three phase signals
init_kalman = struct;
%% Constants, should not be necessary to change these
init_kalman.eps_adaptive = 1e-10;
init_kalman.N_iterations= 10;
init_kalman.ang_bias = -pi/2;
%% From input
init_kalman.hp = hp;
init_kalman.hn = hn;
init_kalman.Np = length(hp);
init_kalman.Nn = length(hn);
init_kalman.N = init_kalman.Np + init_kalman.Nn;
init_kalman.Q = Q0;
init_kalman.R = R;
init_kalman.P0 = P;
init_kalman.x0 = x0;
init_kalman.eye2N = eye(2*init_kalman.N);
end
```

B.4 Harmonics linearization mapping method

```
syms m
```

```
F=1000;           %mapping frequency range
f1=50;            %fundamental frequency
R=10;             %Resistor
C=0.0003;         %capacitor
L1=5e-3;          %inductor 1
L2=5e-3;          %inductor 2

Zdc=@(w)((L2*w+1/(C*w+1/(R+L1*w))));     %dc impedance model

s_p=zeros(1,F);
amp_p=zeros(1,F);
s_n=zeros(1,F);
amp_n=zeros(1,F);
s_dc=zeros(1,F);
amp_dc=zeros(1,F);

for j=1:F
    for m=-1000:1000
    s_p(j) =s_p(j) + 1/((1-36*m^2)*(Zdc(i*12*pi*m*f1))) + ...
        1/((1-6*m^2)*(Zdc(2*pi*j*i+i*2*pi*(6*m-1)*f1)));
    s_n(j) =s_n(j) + 1/((1-36*m^2)*(Zdc(i*12*pi*m*f1))) + ...
        1/((1+6*m^2)*(Zdc(2*pi*j*i+i*2*pi*(6*m+1)*f1)));
    end
    amp_p(j)=abs((pi^2/9)*s_p(j)^(-1));
    amp_n(j)=abs((pi^2/9)*s_n(j)^(-1));
    s_dc(j)=Zdc(i*2*pi*j);
    amp_dc(j)=abs(s_dc(j));
end
figure
semilogx(1:F, amp_p(1:F),1:F, amp_n(1:F))
title('Impedance')
xlabel('frequency[Hz]'), ylabel('Magnitude')
legend('positive','negative')
```

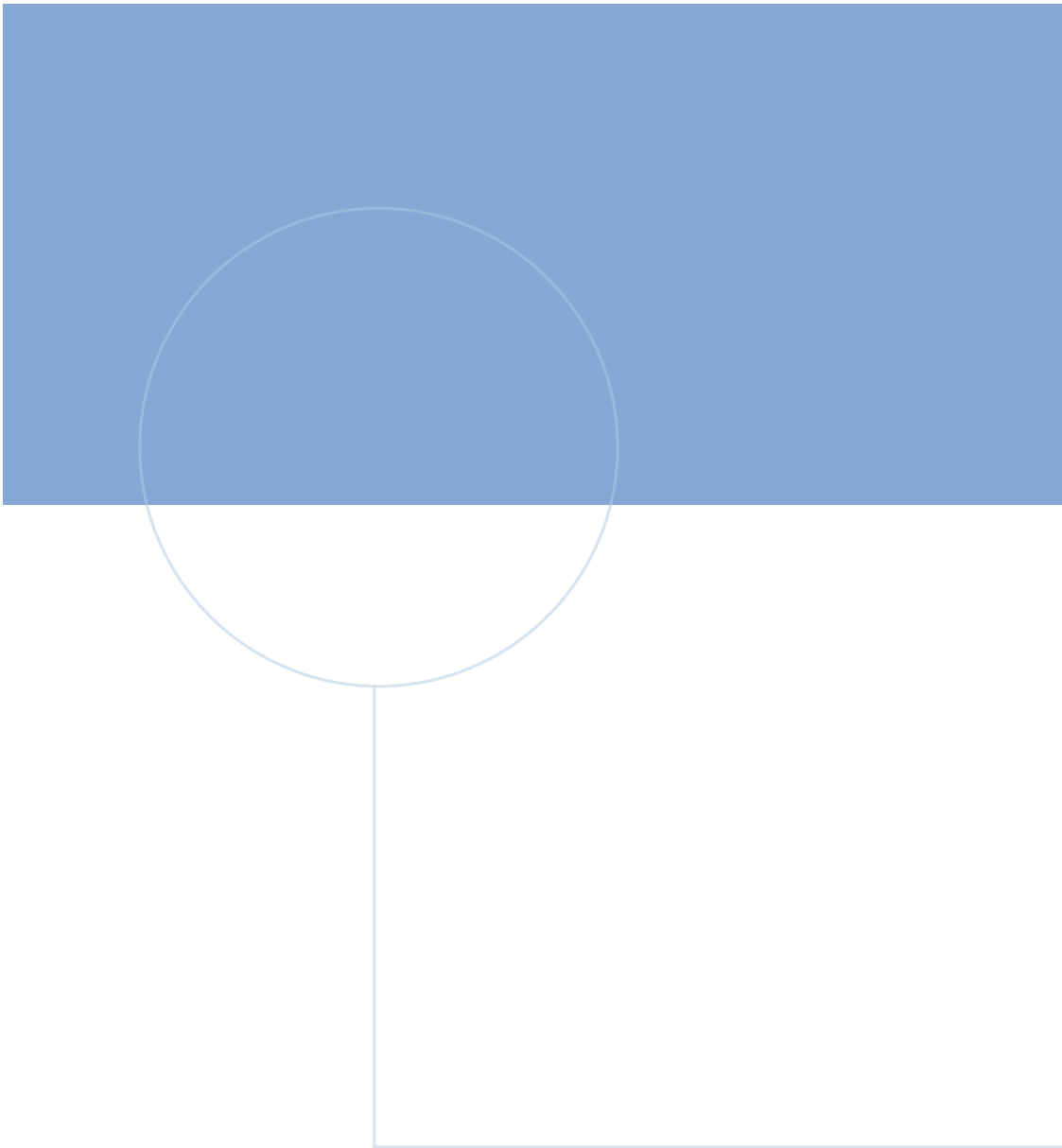

NTNU
Norwegian University of
Science and Technology